

Electrochemical Analysis of H₂S Corrosion on 13% Chromium Stainless Steel

By **Mohammed Abdul Rahman**

Thesis submitted

to the School of Graduate Studies in partial fulfillment of the
requirements for the degree of

Master of Engineering

(Department of Mechanical Engineering)

Faculty of Engineering and Applied Sciences

Memorial University of Newfoundland

May 2018

St. John's Newfoundland and Labrador

“Dedicated to my parents

Mohammed Abdul Qayoom Basith and Nasreen Sultana”

ABSTRACT

The chemical reactions between steel and a corrosive environment cause severe corrosion, which has become a significant concern for the oil and gas industry due to the increase in the number of oil field shutdowns and equipment failures as the exploration of sour oil fields has considerably increased in the last decade. This research studies the effect of the hydrogen sulphide (H₂S) environment on 13% chromium stainless steel, one of the most commonly used corrosion resistant alloy in the oil industry for sour oil fields containing hydrogen sulphide. The corrosion behaviour, including corrosion rates, the effect of environmental conditions and the formation of protective films, were examined during the study. A series of experiments was performed using the conventional electrochemical method to study the effects of temperature, pH and immersion time on the corrosion behaviour of 13% chromium stainless steel in the H₂S environment. Corrosion behaviour was monitored using the polarisation resistance technique. A scanning electron microscope (SEM) equipped with energy dispersive X-ray spectroscopy (EDS) was used to conduct morphological characterization and X-ray diffraction (XRD) was used to study the crystal structure of corrosion products. This study shows that each environmental parameter has a significant impact on corrosion behaviour.

ACKNOWLEDGEMENTS

I appreciate and would like to thank my supervisor, Dr. John Shirokoff, for his dedication, direction, and supervision of my research and academic life. His excellent guidance has helped me complete my thesis.

Many people have helped me during this research period. Firstly, I would like to thank Mr. Steve Steele for assisting me in using the corrosion laboratory. Also, I would like to extend my appreciation to Dr. David Grant and Dr. Wanda Alyward for their help with the SEM and XRD equipment.

I appreciate Dr. Ali Nasiri for his comments during my experimental setup and Ladan Khaksar (Ph.D. student) for helping me during the beginning of my research.

I would also like to thank my friend Shams Anwar (Ph.D. student) for helping me write a MATLAB code to generate graphs.

I am grateful for the financial support provided by Memorial University of Newfoundland and Suncor Energy.

I am considerably indebted to my family members, especially my parents, for their support and understanding.

Finally, I would like to thank all my friends and colleagues.

TABLE OF CONTENTS

ABSTRACT.....	ii
ACKNOWLEDGMENTS	iii
TABLE OF CONTENTS.....	iv
LIST OF TABLES	vii
LIST OF FIGURES	viii
ABBREVIATIONS	xi
NOMENCLATURE	xiii
1. INTRODUCTION	1
1.1. Overview	1
1.2. Research objective	2
1.3. The organization of thesis	2
2. INSTRUMENTATION	4
2.1. Potentiostat.....	4
2.2. Scanning electron microscope (SEM).....	5
2.3. Energy dispersive X-ray spectroscopy (EDS).....	6
2.4. X-ray diffraction (XRD)	7

3. LITERATURE REVIEW	9
3.1. Sour oil field exploration	9
3.2. Corrosion problems in sour oil field exploration	9
3.3. Corrosion resistant alloys used in sour oil field exploration.....	10
3.4. Hydrogen sulphide	11
3.4.1. Hydrogen sulphide corrosion.....	12
3.4.2. Effect of temperature.....	13
3.4.3. Effect of pH.....	13
3.4.4. Effect of hydrogen sulphide concentration.....	13
3.4.5. Effect of immersion time.....	14
3.5. Corrosion product layers in hydrogen sulphide environment	14
3.6. Electrochemical methods	16
3.6.1. Galvanic corrosion.....	16
3.6.2. Linear polarisation resistance.....	16
3.6.3. Potentiodynamic polarisation technique	19
4. EXPERIMENTAL SETUP.....	22
4.1. Experimental details.....	22
4.2. The Pourbaix diagram of the chemical bath.....	25
4.3. Surface morphology observation and corrosion product analysis.....	27

5. RESULTS AND DISCUSSION.....	28
5.1. Effect of temperature on the corrosion behaviour of 13% chromium stainless steel.....	28
5.2. Corrosion rate with respect to the change in temperature.....	31
5.3. Effect of pH on the corrosion behaviour of 13% chromium stainless steel.....	32
5.4. Corrosion rate with respect to the change in pH value	35
5.5. Effect of immersion time on the corrosion behaviour of 13% chromium stainless steel...36	
5.6. Corrosion rate with respect to the change in immersion time.....	39
5.7. Scanning electron microscope (SEM) and Energy dispersive X-ray spectroscopy (EDS)	41
5.8. X-ray diffraction (XRD)	48
6. CONCLUSION.....	51
7. FUTURE WORK AND RECOMMENDATIONS.....	52
REFERENCES	53
APPENDIX.....	60

LIST OF TABLES

Table 4.1.1	Experimental parameters	22
Table 4.1.2	The chemical composition of the specimen.....	22
Table 4.1.3	Bath compositions for the corrosion film formation on the steel substrate.....	23
Table 4.2.1	List of the conditions for experimental parameters	26

LIST OF FIGURES

Figure 2.2.1 Sample image of Scanning electron microscope (SEM image of Iron sulphide layer).....	5
Figure 2.3.1 Sample image of EDS showing the composition of Iron sulphide layer on the steel surface.....	6
Figure 2.4.1 XRD pattern of the corrosion sample.....	7
Figure 3.6.2.1 Linear polarisation resistance curves.....	17
Figure 3.6.3.1 Anodic polarisation scan for stainless steel.....	19
Figure 3.6.3.2 Cathodic polarisation scan for stainless steel.....	20
Figure 4.1.1 Iron (II) chloride solution.....	24
Figure 4.1.2 Urea solution.....	24
Figure 4.1.3 Thioacetamide solution.....	24
Figure 4.2.1 Pourbaix diagram for steel substrate immersed in a chemical bath.....	25
Figure 5.1.1 Polarisation curves of 13% chromium stainless steel at different temperatures: 40°C and 50°C at pH2.....	28
Figure 5.1.2 Polarisation curves of 13% chromium stainless steel at different temperatures: 50°C and 70°C at pH2.....	29

Figure 5.1.3 Polarisation curves of 13% chromium stainless steel at different temperatures: 40°C and 70°C at pH3	30
Figure 5.2.1 Corrosion rates measured at different temperatures having the same pH and immersion time.....	31
Figure 5.3.1 Polarisation curves of 13% chromium stainless steel at different pH values: pH2 and pH3 at 40°C	32
Figure 5.3.2 Polarisation curves of 13% chromium stainless steel at different pH values: pH2 and pH3 at 70°C	33
Figure 5.3.3 Polarisation curves of 13% chromium stainless steel at different pH values: pH4 and pH5 at 80°C	34
Figure 5.4.1 Corrosion rates measured at different pH values having the same temperature and immersion time.....	35
Figure 5.5.1 Polarisation curves of 13% chromium stainless steel at different immersion times: 24 hours and 48 hours at pH2, 40°C	36
Figure 5.5.2 Polarisation curves of 13% chromium stainless steel at different immersion times: 24 hours and 48 hours at pH3, 40°C	37
Figure 5.5.3 Polarisation curves of 13% chromium stainless steel at different immersion times: 24 hours and 48 hours at pH3, 80°C	38
Figure 5.6.1 Corrosion rates measured at different immersion times having the same temperature and pH value	39

Figure 5.7.1 SEM images and EDS analysis of the corrosion products formed on the steel surface for (a) original uncorroded sample (b) pH2, 50°C, 24 hours (c) pH2, 70°C, 24 hours 42

Figure 5.7.2 SEM images and EDS analysis of the corrosion products formed on the steel surface for (d) pH3, 40°C, 48 hours (e) pH3, 70°C, 48 hours (f) pH4, 80°C, 48 hours..... 43

Figure 5.7.3 SEM images and EDS analysis of the corrosion products formed on the steel surface for (g) pH5, 80°C, 48 hours (h) pH6, 50°C, 24 hours (i) pH6, 50°C, 48 hours..... 45

Figure 5.8.1 XRD analysis of the corrosion product formed on the steel surface for (a) pH2, 40°C, 24 hours (b) pH2, 40°C, 48 hours (c) pH2, 40°C, 72 hours (d) pH2, 70°C, 24 hours..... 48

Figure 5.8.2 XRD analysis of the corrosion product formed on the steel surface for (e) pH3, 70°C, 72 hours (f) pH4, 80°C, 48 hours (g) pH5, 80°C, 72 hours (h) pH6, 50°C, 24 hours 50

ABBREVIATIONS

BCC	Body Center Cubic
CAMI	Coated Abrasive Manufacturers Institute
CE	Counter Electrode
RE	Reference Electrode
WE	Working Electrode
CR	Corrosion Rate
CRA	Corrosion Resistant Alloy
EDS	Energy Dispersive X-ray Spectroscopy
ICDD	International Center for Diffraction Data
JCPDS	Joint Committee on Powder Diffraction Standards
LPR	Linear Polarization Resistance
NACE	National Association of Corrosion Engineers
OCP	Open Circuit Potential
PDF	Powder Diffraction Files
SEM	Scanning Electron Microscope
HIC	Hydrogen-Induced Cracking
SSC	Sulfide Stress Cracking

SOHIC Stress-Oriented Hydrogen Induced Cracking

XRD X-ray Diffraction

NOMENCLATURE

M Molar

g Gram

L Litre

A Ampere

mA Mili Ampere

nA Nano Ampere

°C Degrees Celsius

V Voltage

i Current

S Second

pH Measure of hydrogen ion concentration

mm Millimeter

cm Centimeter

h Hour

E Potential

E_{corr} Corrosion potential

I_{corr} Corrosion current

1. INTRODUCTION

1.1 OVERVIEW

Oil and gas exploration in highly corrosive environments has significantly increased in recent years, making hydrogen sulphide (H_2S) corrosion an important topic of research after several pipeline failures and due to the safety risks associated with this dangerous gas. Compared to the number of studies on carbon dioxide (CO_2) corrosion, there is a limited amount of experimental work available on hydrogen sulphide (H_2S) corrosion, due to the difficulty in working with hydrogen sulphide gas [1]. Corrosion resistance alloys (CRA) are used in the H_2S environment due to the passive film formation along with the self-repair nature of those passive films, but these CRA started corroding once these passive layers stopped forming efficiently [2]. The internal corrosion of the corrosion resistant alloys is controlled by environmental parameters such as temperature, pH value, the concentration of H_2S in the environment and its immersion time. A minute change in any of these parameters can cause severe corrosion, causing catastrophic damages leading to the shutdown of the oilfields. The formation and growth of corrosive films on the steel surface are directly dependent on these environmental parameters. In some extreme conditions, the formed corrosion film is not sufficient to protect the underlying steel, which initiates localized corrosion with high corrosion rates, and very little research has been done related H_2S corrosion in the oil industry [3][4].

Another corrosion concern in the industry is the transportation of the oil and gas. Supply of oil and gas in huge volumes are being done by pipelines since many decades, as a reliable and economical method. To achieve the requirements for oil and gas, these pipelines run hundreds of kilometers and corrosion makes it difficult to maintain the integrity of such large networks. This transportation is commonly in multiphase form, which contains gases such as CO_2 , H_2S , and a few other particles

in the transmission pipelines, these gases and particles will accelerate the corrosion rate of the pipeline [5]. The corrosion cost has increased to by millions of dollars in recent years [6].

1.2 RESEARCH OBJECTIVE

This research aims to understand the electrochemical behaviour of the most commonly used corrosion resistant alloy (CRA) in H₂S environments, which is 13% chromium stainless steel. This study includes the corrosion behaviour with the changes in environmental parameters, corrosion rates for different conditions, the growth of sulphide films under each condition and the impact of these protective films. This goal will be achieved by investigating a steel sample placed in an electrochemical cell with different experimental parameters and analyzing the sample after specific immersion times using the polarisation resistance technique. The morphological properties and crystalline phase structure of the sample are examined by scanning electron microscope (SEM) installed with energy dispersive spectroscopy (EDS) and X-ray diffraction (XRD).

1.3 ORGANISATION OF THESIS

This thesis is organized into six chapters which include Introduction, Literature review, Experimental details, Results and discussions, Conclusion and Future works.

Chapter 1: Introduction, introduces the background and current problems in the oil and gas industry regarding H₂S corrosion, the objective of this research and its organization.

Chapter 2: Instrumentation, describes the instruments used in this research work, such as the Potentiostat, SEM, EDS and XRD.

Chapter 3: Literature Review, reviews oil fields' exploration and encountering of corrosive gases, the corrosion problems in the sour oil fields and currently used corrosion resistant alloys. The techniques and methods used to conduct the experiments are also discussed.

Chapter 4: Experimental details, introduces the experimental setup, the bath preparation, the electrochemical setup and various parameters used to conduct different experiments.

Chapter 5: Results and discussion, focuses on the results obtained by experiments and the analysis of a sample using various techniques and equipments. It also discusses the obtained results in the form of discussion.

Chapter 6: Conclusion, summarises the results of this research and draws a major conclusion from the obtained findings.

Chapter 7: Future work, suggests the way to further this research work and its findings.

2 INSTRUMENTATION

In this research, the instruments needed for the experimentation and characterization of samples include the Potentiostat, Scanning Electron Microscope (SEM), Energy Dispersive X-ray Spectroscopy (EDS) and X-ray diffraction (XRD).

2.1 POTENTIOSTAT

A potentiostat is a simple device that depends on operational amplifiers to maintain a desired potential difference between two electrodes (working and reference electrodes) immersed in a solution while recording the electrical current that flows between them. Usually, a third electrode (counter electrode) is added to the system to isolate the electrode used as a potential reference (reference electrode) from the charge transfer reaction. The potentiostat applies a voltage and records the current response that is characteristic of the test's sample [7].

The counter electrode (CE) (also known as an auxiliary electrode), is an electrode which is used to close the current circuit in the electrochemical cell. It is typically made of an inert material (e.g. Pt, Au, graphite, glassy carbon) and generally, it does not contribute to the electrochemical reaction. Since the current is flowing between the WE and the CE, the total surface area of the CE should be higher than the area of the WE. Therefore, it will not be a limiting factor in the kinetics of the electrochemical process under examination [8].

The reference electrode (RE) is an electrode with a stable and well-known electrode potential and is used as a point of reference in the electrochemical cell for the potential control and measurement. The high stability of the RE potential is usually attained by retaining a redox system with constant concentrations of each participant of the redox reaction [9]. The current flow through the RE is

kept close to zero, attained by using the CE to close the current circuit in the cell together with a high input impedance on the electrometer (>100 GOhm).

The working electrode (WE) is the electrode in an electrochemical system on which the reaction of attention is taking place. Regular WE can be made of inert materials such as gold (Au), silver (Ag), platinum (Pt), glassy carbon (GC) and mercury (Hg) drop and film electrodes. For corrosion applications, the material of the WE is the material under investigation. The size and shape of the WE can also differ, depending on the application [10], [11].

2.2 SCANNING ELECTRON MICROSCOPE (SEM)

Scanning Electron Microscope is used to study the morphological characterization of the corrosion product formed on the steel surface. It shows a magnified image of the corrosion product, providing key insights about the corrosion film and its thickness.

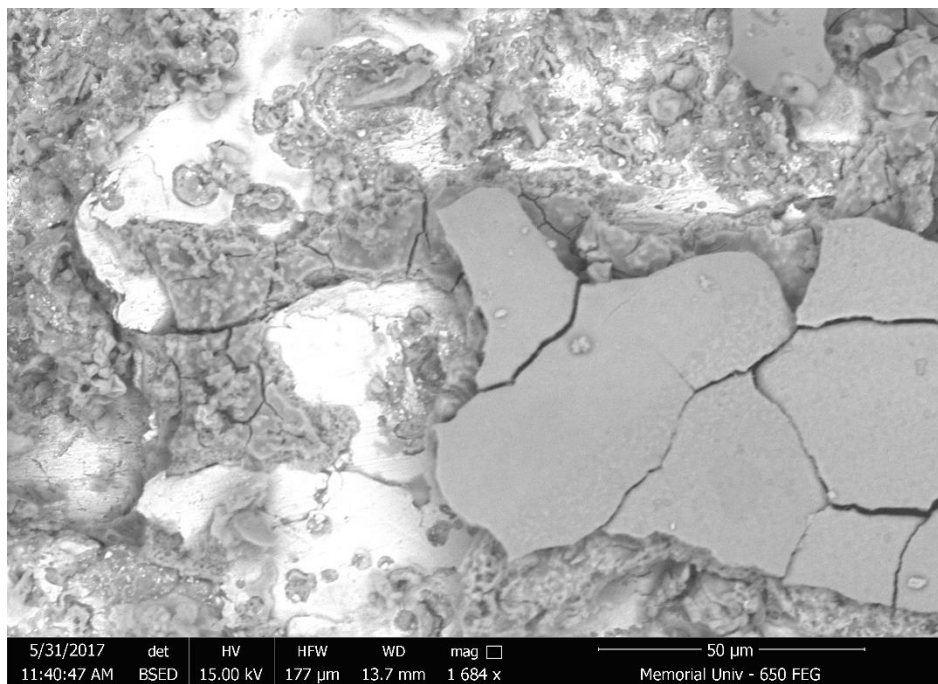


Figure 2.2.1 Sample image of Scanning electron microscope (SEM image of Iron sulphide layer).

SEM takes images by scanning the surface with a high beam of electrons. These electrons interact with the atoms in the steel and send back various signals. These signals contain key morphological and qualitative composition information of the sample's surface which generate high-resolution images known as SEM images [12].

The sample must be electrically conductive to be operational with the SEM equipment.

2.3 ENERGY DISPERSIVE X-RAY SPECTROSCOPY (EDS)

Energy dispersive X-ray spectroscopy, also known as EDS. It is mostly equipped with SEM and is a tool for compositional analysis of the sample's surface along with the SEM image.

During this analysis, a high beam of charged electrons or an X-ray beam is bombarded on the sample surface. This bombardment displaces the inner shell electrons at the focus point and excites them to the outer shell, emitting back rays which are measured using a spectrometer, resulting in the compositional information of the focused sample as shown in figure 2.3.1.

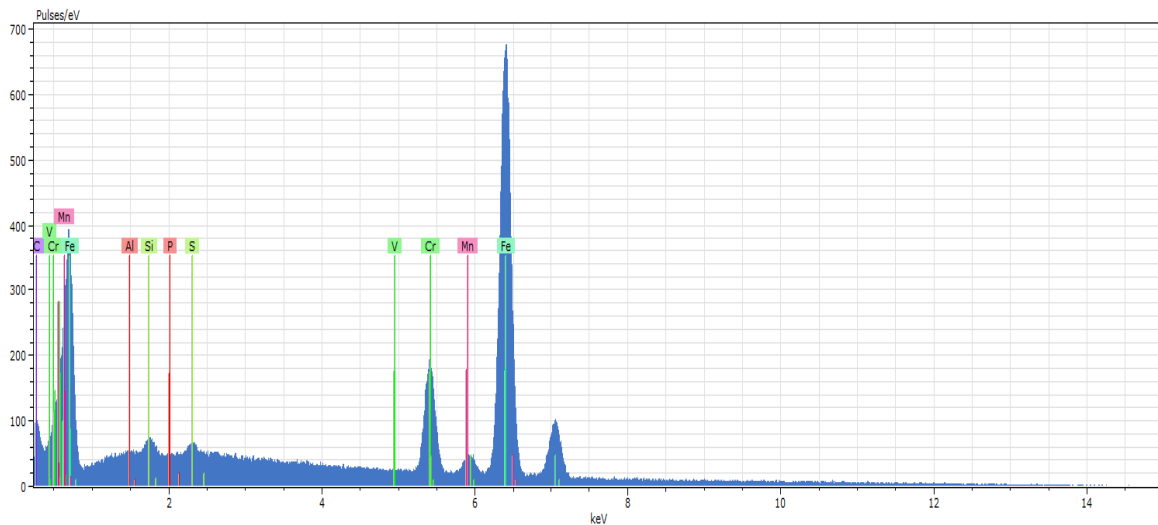


Figure 2.3.1. Sample image of EDS showing composition of Iron sulphide layer formed on the steel surface.

The principle of this method is that each element has a unique atomic structure corresponding to the X-ray emission spectrum which helps in identification of the element and its quantitative analysis. This sometimes makes it difficult to accurately identify and analyze the sample surface [13].

2.4 X-RAY DIFFRACTION (XRD)

X-ray diffraction (XRD) is used for characterization of the composition of the sample surface and to identify its crystal structure and phase.

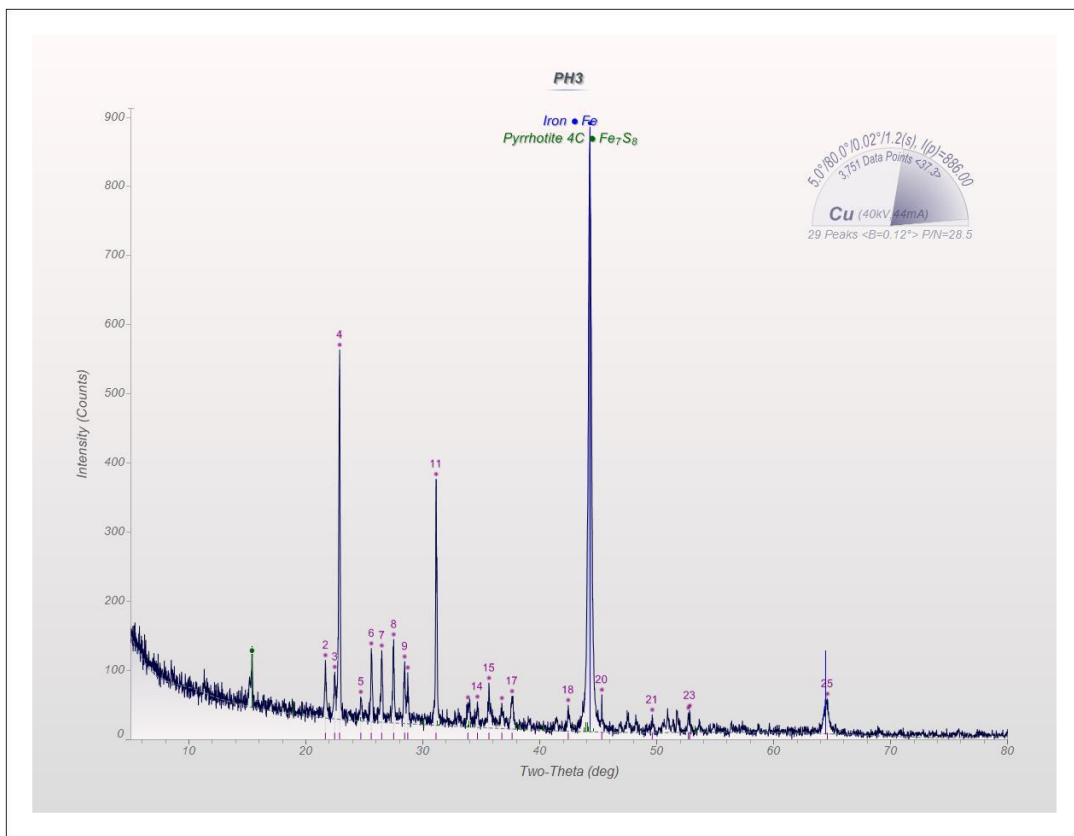


Figure 2.4.1 XRD pattern of a corrosion sample.

During this procedure, X-ray beams generated from different angles are focused on the sample surface. When the X-ray encounters the unique crystal structure on the sample, it becomes diffracted, making an XRD pattern. This unknown pattern is then compared in the database with similar peaks, which can determine the phase and crystal structure of the sample surface[13].

3 LITERATURE REVIEW

3.1 SOUR OIL FIELD EXPLORATION

The exploration of sour oil and gas fields has significantly increased throughout the world, especially in an extremely corrosive oil field, including production and transportation, has become a significant concern to the industry due to corrosive environments in sour fields, which cause material damage and continuous shutdowns [14].

Safety standards call attention to the danger of exposure to harmful gases, mainly hydrogen sulphide (H_2S) present in this type of oil fields. Gases found in sour oil fields are detrimental to humans. With H_2S gas, a low concentration of 10 ppm is sufficient to cause stress in human beings, and a concentration of 250ppm quickly leads to death [15].

In sour oil production fields, elemental sulphur deposition appears in the fields with high H_2S concentration. H_2S is more soluble in the aqueous state compared to other gases found in sour oil fields. This solid elemental sulphur contacts the steel in the aqueous state, causing severe corrosion damage to the pipelines. Sour oil corrosion damage has become a major issue in the industry and researchers are still uncertain about the corrosion mechanism of sour oil fields [16], [17].

3.2 CORROSION PROBLEMS IN SOUR OIL FIELD EXPLORATION

The harmful gases causing severe corrosion problems in sour oil fields are naturally occurring components of oil and gas and are impenetrable in the rocks during the geothermal changes over an extended period. The corrosion in sour oil fields is a source of problems for production, including reduced material strength, equipment failures, leakages and changes in the surface properties [18]. H_2S leads to embrittlement of carbon steel; forms of embrittlement caused by H_2S

are hydrogen induced cracking (HIC), sulphide stress cracking (SSC), and stress-oriented hydrogen induced cracking (SOHIC).

Hydrogen-Induced Cracking (HIC): In this type of embrittlement, hydrogen is absorbed from the aqueous environment, leaving traces of hydrogen on the steel surface which develops pressure and starts to crack the steel surface.

Sulphide Stress Cracking (SSC): The environmental H₂S diffuses hydrogen through a chemical reaction and attacks the stress-induced areas of the steel surface such as the welded joints. The chemically released hydrogen starts to form on the stressed areas of the steel surface, initiating cracks and embrittlement in a direction perpendicular to the stress.

Stress-Oriented Hydrogen Induced Cracking (SOHIC): This is typically a combination of HIC and SSC, where cracks form perpendicularly to the stress, with a combination of hydrogen induced cracks on the base metal surface [19][20].

3.3 CORROSION RESISTANT ALLOYS USED IN SOUR OIL FIELDS EXPLORATION

In a harsh corrosion environment, the low alloy tubular steel has to be changed after a certain period due to the corrosion of steel in extreme environmental conditions, especially with high temperatures. This practice is costly to the oil and gas industry.

The finished product of a chemical reaction in an H₂S aqueous medium on the steel surface is written as:



Therefore, the corrosive H₂S media in contact with steel form different corrosive layers of the iron and sulphur anionic surface [21]. These corrosion products have a catastrophic effect on the low alloy steel over a period. Therefore, to minimize the expenses, an alternative has been used to counter the corrosion of the low alloy steel. The corrosion resistant alloys (CRA) were recommended for tubular use in sour oil fields, they perform slightly better than flat alloy steel due to the improved chemical composition. The CRA show improvement in withstanding the severe corrosion in different environmental conditions.

The alloys satisfactory for the H₂S environment are the steels with high contents of chromium (Cr), molybdenum (Mo) or nickel (Ni). These alloys resist different types of corrosion in sour conditions compared to flat alloy steels. The detailed outline for the selection of corrosion resistant alloys in the H₂S environment is recommended in part 3 of NACE MRO175/ISO1516-3[22], [23], [24].

3.4 HYDROGEN SULFIDE (H₂S)

Hydrogen sulphide (H₂S) is a colourless, toxic and highly flammable gas with the odour of rotten eggs. It occurs naturally in different environments such as sewers, volcanoes, oil and gas and in some water wells. Human exposure to H₂S gas may cause a severe headache, nausea, eye irritation and insomnia. Exposure to high concentrations can cause loss of consciousness and eventually, death due to respiratory paralysis [25], [26], [27].

The detection of H₂S is enabled by the sensor using different techniques. A risky manual method to detect H₂S is by exposing a paper soaked in lead acetate to the area, the presence of H₂S turns the paper black. The most common in-situ H₂S sensor are the thermal conductivity detectors, flame photometric detectors and sulphur chemiluminescence detectors [28].

3.4.1 HYDROGEN SULPHIDE CORROSION

Several studies have been conducted to study H₂S corrosion in oil pipelines and the reaction between hydrogen sulphide (H₂S) and water (H₂O) is complicated.

The stability of different H₂S corrosion products or the sulphur species (S²⁻ or HS⁻) is dependent on environmental conditions such as temperature, pH and concentration of H₂S. In an H₂S environment, the different types of corrosion products commonly formed are Mackinawite, Pyrrhotite, Troilite, Pyrite, Greigite and Marcasite.[29], [14].

This chemically deposited iron sulphide layer (Fe_xS_y) on the steel surface limits further corrosion by protecting the steel from exposure to the H₂S environment. The first iron sulphide product to form is Mackinawite, a fragile product due to its sulphur deficiency, and with an increase of immersion time, mackinawite break and leads to an increase of the corrosion rate and later, the formation of stable corrosion products[30].

The dissolution of iron sulphide for the film formation can be explained as [31]:





3.4.2 EFFECT OF TEMPERATURE

Temperature has a direct impact on the formation of corrosion products, which in turn changes the rate of corrosion and type of corrosion associated with a change in temperature. The impact of temperature has a severe effect over a short period and over long exposure, the temperature does not have an enormous effect on the H₂S corrosion. The behaviour of corrosion is directly dependent on iron sulphide formation [32]. An increase in temperature up to 80°C can increase the rate of deposition on the steel surface [33].

3.4.3 EFFECT OF pH

The passive nature and the type of iron sulphide mineral formation are significantly dependent on the pH value. At lower pH values such as pH 2, the solubility of iron sulphide phases increase, which dissolves iron and sulphide has a minimal effect on the precipitation on the steel surface. However, with the rise in pH values such as a pH (3-5), the formation of iron sulphide passive films increases on the steel surface, which inhibits the effect of H₂S [34].

3.4.4 EFFECT OF H₂S CONCENTRATION

The concentration of H₂S has an immense effect on the corrosion behaviour of metal. In environments with higher H₂S concentration, the passive layers of iron sulphide films are loosely packed, and the formation of blisters leads to a decrease in the protective ability of the passive film [35].

3.4.5 EFFECT OF IMMERSION TIME

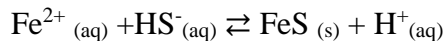
The efficacy of a protective barrier of corrosion products in the H₂S environment depends on the immersion time. As the immersion time increases, the passivation decreases, resulting in weak adherence of the corrosion film to the steel surface. With an increase in immersion time, the passive layer starts to break, which in turn exposes the surface of the steel to the harsh environment [36], [37].

3.5 CORROSION PRODUCT LAYER IN H₂S ENVIRONMENT

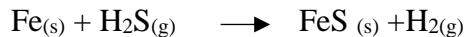
The rate of corrosion is highly dependent on the type of corrosion product formed on the steel surface. The rate of film formation of the corrosive products and the precipitation rate of these films depend on several factors, most importantly on the concentration of H₂S and the pH of the environment; different films can be formed based on their composition. The protective nature of these films determines the rate of corrosion in the metal [38].

Corrosion product formed in the H₂S environment are minerals of iron sulphide (FeS). These iron sulphide films develop either due to precipitation or by direct chemical reaction between the sour environment and iron (Fe)[35], [39].

The formation of FeS by precipitation:



FeS formed by direct chemical reaction



The different types of FeS films to form on the surface as corrosion products depend on the surrounding environmental conditions. There are six different types of naturally occurring FeS

minerals: mackinawite (Fe_{1+x}S), pyrrhotite (Fe_{1-x}S), greigite (Fe_3S_4), smythite (Fe_9S_{11}), marcasite (FeS_2), and pyrite (FeS_2) [40].

Mackinawite: Mackinawite is a sulphur deficient iron sulphide. The formula for mackinawite is Fe_{1+x}S where 'x' ranges between 0.057 to 0.064. Mackinawite has a two-dimensional stacked FeS structure, and it is the first corrosion product to form in low H_2S concentrations as it is thermodynamically unstable and can be converted to other FeS minerals with the addition of sulphur content [40], [41].

Pyrrhotite: Pyrrhotite is an iron deficient iron sulphide. The formula for pyrrhotite is Fe_{1-x}S . It is also called Troilite [42].

Greigite: Greigite is named after a mineralogist, Joseph W. Greig. The formula for Greigite is Fe_3S_4 . It is isostructural, and it is ferromagnetic and semi-conductive [43], [44].

Marcasite: This is also called white iron pyrite. The formula of marcasite is FeS_2 and has an unstable crystalline structure which tends to change with the changes in the environment [13].

Pyrite: Pyrite has a cubic crystal structure and is also called fool's gold. Its formula is FeS_2 and forms with a high content of sulphur. The structure of pyrite is found to be stable compared to other H_2S minerals.

When these protective films start to break from the surface of the steel, localized corrosion starts to occur, which forms permanent anodic and cathodic sites on the surface [45], [46]. Environmental conditions such as temperature, pH, elemental sulphur, flow etc. play a significant role in these processes and some research suggests chlorine ions influence the localized corrosion in H_2S systems [47]. Despite a great deal of research, the mechanism of H_2S corrosion is inadequately understood.

3.6 ELECTROCHEMICAL METHODS

3.6.1 GALVANIC CORROSION

Galvanic corrosion occurs between two different metals in an electrochemically active medium. In galvanic corrosion, the more noble metal becomes cathodic and starts to corrode the less noble metal, especially in a corrosive environment. Mostly, galvanic corrosion is even and localized at junctions, depending on the type of alloy and the corrosive medium. If the protective film is not formed, the corrosion will be severe and becomes chemically difficult.

When two metals are connected electrically in a corrosive medium, the difference between their corrosion potential will cause the corrosion to initiate both oxidation and reduction processes. Corrosion potential can determine the nobility of the metal. Hence, the metal which is less noble will become more anodic, and the metal which is nobler will be cathodic, forming a galvanic series based on the nobility of the metal. The metal placed at the opposite ends of the galvanic series will have very high corrosion rate, as one metal is very anodic, and the other metal is very cathodic. The anodic metal will be electrochemically corroded in the corrosive medium by chemical reactions, wear and migration of ions from the less noble metal towards the more noble metal; by this transfer of ions, the more noble metal will become more protective against corrosion in the corrosive medium. To measure the current galvanic current between two dissimilar metals, a zero resistance ammeter (ZRA) is used [48].

3.6.2 LINEAR POLARISATION RESISTANCE

Linear polarisation resistance (LPR) is an electrochemical method to determine the reactions in an electrolytic solution. Corrosion rates and the exchange of current densities can be specified in an electrochemical experiment using LPR.

The term 'polarising the electrode' is used in an open circuit when the potential of an electrode is changed from its original value. In this polarisation of an electrode in the electrochemical reaction, the flow of current takes place starting from the surface of an electrode. This current flow is controlled by the kinetics of the reaction and the reactant's diffusion.

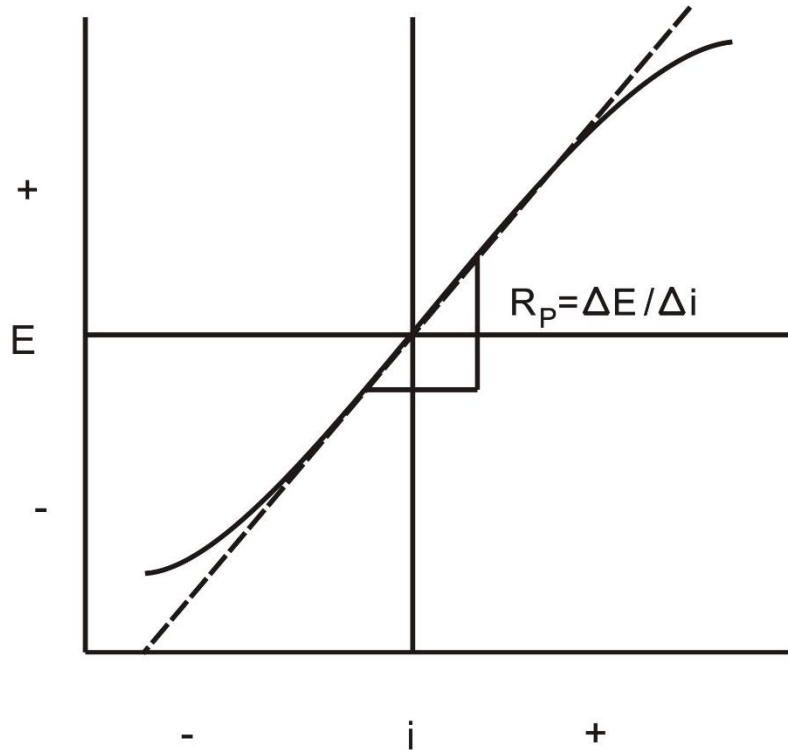


Figure 3.6.2.1 Linear Polarisation Resistance curve.

In an open circuit, the equilibrium between the two electrochemical reactions controls the open circuit potential (OCP) when an electrode undergoes uniform corrosion.

When the OCP has equal cathodic and anodic potentials, it is called a mixed potential, and the value of the current for any reaction is called the corrosion current (I_{corr}).

$$I = I_{corr} \left(e^{\frac{2.303(E-E_{ocp})}{\beta_a}} - e^{\frac{2.303(E-E_{ocp})}{\beta_c}} \right)$$

where:

I = measured current (amperes)

I_{corr} – corrosion current (amperes)

E_{ocp} – Open circuit potential (volts)

β_a – Anodic beta coefficient (volts/decade)

β_c – Cathodic beta coefficient (volts/decade)

If a small signal is applied, the above equation can be written as:

$$I_{corr} = \frac{\beta_a \beta_c}{2.303(\beta_a + \beta_c)} * \frac{1}{R_p}$$

where:

R_p = Polarisation resistance

Once Tafel constants are known, I_{corr} can be calculated, which is used to calculate the corrosion rate.

3.6.3 POTENTIODYNAMIC POLARISATION TECHNIQUE

Potentiodynamic polarisation is a technique to measure the polarization resistance in which the rate of electrode potential is varied by the application of a current through the electrolyte. This technique is used in the polarization of metal specimen for testing the corrosion.

In Potentiodynamic experiments, the current represents the rate with which the anodic and cathodic reactions are taking place on the working electrode (WE), and cathodic currents are considered to be negative, and anodic currents to be positive. In general, the current is expressed in terms of the current per unit area of the WE, or the current density. It is noticeable that in an Evans diagram (a plot of E vs $\log(I)$) the complete current density values are plotted it means that, both anodic and cathodic currents are plotted as positive values.

Anodic Scan:

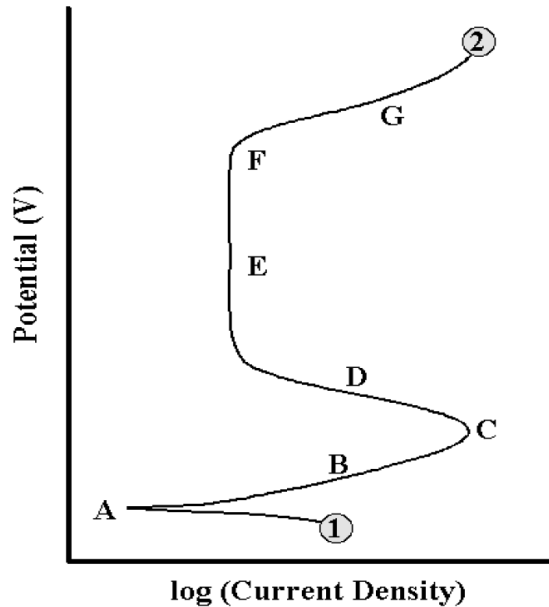


Figure 3.6.3.1 Anodic polarization for stainless steel

A standard schematic anodic scan for stainless steel as shown in Figure 3.6.3.1 The scan rate starts from point 1 and progress in the positive potential direction until the termination at point 2. The OCP is located at point A. At this potential summation of anodic and cathodic reaction rates on the electrode surface is zero. The region B is the active region. Point C is known as passivation potential, and as the applied potential increases above this value then the current density is seen to be decreased with increasing potential (region D) until a low passive current density is attained (passive region-region E). Once the potential has reached a suitably positive value (point F, termed as break-even point), the applied current rapidly increases (region G). This increase in current is due to several phenomena, depending on the alloy/environment combinations.

Cathodic Scan:

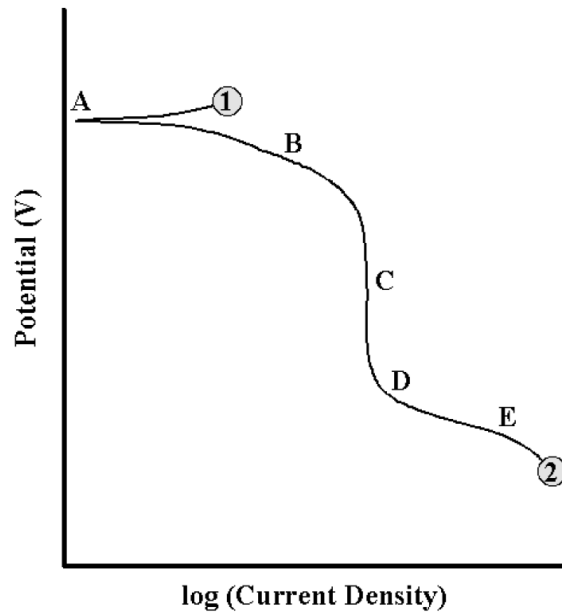


Figure 3.6.3.2 Cathodic polarization scan for stainless steel

A standard schematic cathodic scan for stainless steel as shown in Figure 3.6.3.2. The potential is varied from point 1 and progress in the negative potential direction until the termination at point 2. The OCP is located at point A be determined by the pH and concentration of dissolved oxygen in the solution, region B may represent the oxygen reduction reaction. Further, decrease in the applied potential result in no change in the reaction rate, and thus the measured current remained the same (region C). In the end, the applied potential becomes appropriately negative for another cathodic reaction to becomes effective such as demonstrated at point D. As the potential and driving force becomes very large, this reaction may become dominant as illustrated at point E [38], [64].

4 EXPERIMENTAL SETUP

4.1 EXPERIMENTAL DETAILS

This research aims to study and analyze the behaviour of 13% Chromium stainless steel in the presence of an H₂S environment in different conditions like pH value, temperature and immersion time.

Table 4.1.1 Experimental parameters

Material (Steel Substrate)	13% Chromium stainless steel
Temperature	40°C to 80°C
pH	2 to 6
Immersion time	24 Hrs. to 72 Hrs.

According to NACE MRO175/ISO 15156, the corrosion resistant stainless steel used in the H₂S environment should have a chromium content of 10.5% or more. Therefore, conventional stainless steel with 13% chromium grade 420 has been selected for the experimental work.

Table 4.1.2 The chemical composition of the specimen

<u>Elements</u>	<u>Weight%</u>
Carbon	0.027
Chromium	12
Manganese	0.22
Silicon	0.3
Phosphorous	0.014

Sulphur	0.0035
Vanadium	0.041
Iron	Balance

A conventional three-electrode glass cell setup was used for measuring corrosion rates at different parameters using the polarisation resistance technique, for which a small specimen of steel was used as the working electrode (WE), a graphite rod was used as a counter electrode (CE), and Ag/AgCl/4MKCl sat was used as a reference electrode (RE).

The working electrode was prepared by machining the 13% chromium steel sample to a cylindrical sample piece of the approximate dimension of 1cm length and 1cm diameter. Prior to placing the working electrode into the chemical bath, the working electrode specimen was grinded using sandpaper of grit sizes P220, P320, P400, P600 and micron 6 after which the specimen was immediately cleaned using de-ionized water and dried.

Due to safety concerns associated with H₂S gas, an alternative approach which mimics H₂S gas was used. The chemical bath used in this alternative approach deposits thin films of iron sulphide, exactly as occurs with real H₂S gas [37], [49]. The reagents listed below were mixed with specified concentrations to make the chemical bath.

Table 4.1.3 Bath compositions for the corrosion film formation on the steel substrate

<u>S.No.</u>	<u>Chemical reagents</u>	<u>Chemical formula</u>	<u>Concentrations</u>
1	Iron Chloride (Tetra-hydrate)	FeCl ₂ .4H ₂ O	0.15M
2	Thioacetamide	CH ₃ CSNH ₂	2M

3	Urea	$\text{CH}_4\text{N}_2\text{O}$	1M
---	------	---------------------------------	----

The process of making this chemical bath involves three reagents, i.e. Iron (II) Chloride (0.15M), Urea (1M) and Thioacetamide (2M). Each reagent has to be mixed with de-ionized water, making three different solutions, and each solution has to be stirred at a speed of 350 rpm for approximately 30 minutes.



Figure 4.1.1 Iron (II) Chloride solution

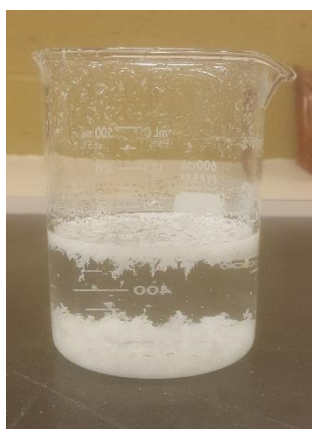


Figure 4.1.2. Urea Solution



Figure 4.1.3. Thioacetamide Solution

These three solutions were mixed and stirred for 2 hours at a speed of 350 rpm so that a homogenous electrolyte solution was achieved. The reaction mechanism involves the release of iron and sulphur ions, which help in the deposition of the iron sulphide (FeS) layer on the working electrode.

4.2 THE POURBAIX DIAGRAM OF THE CHEMICAL BATH

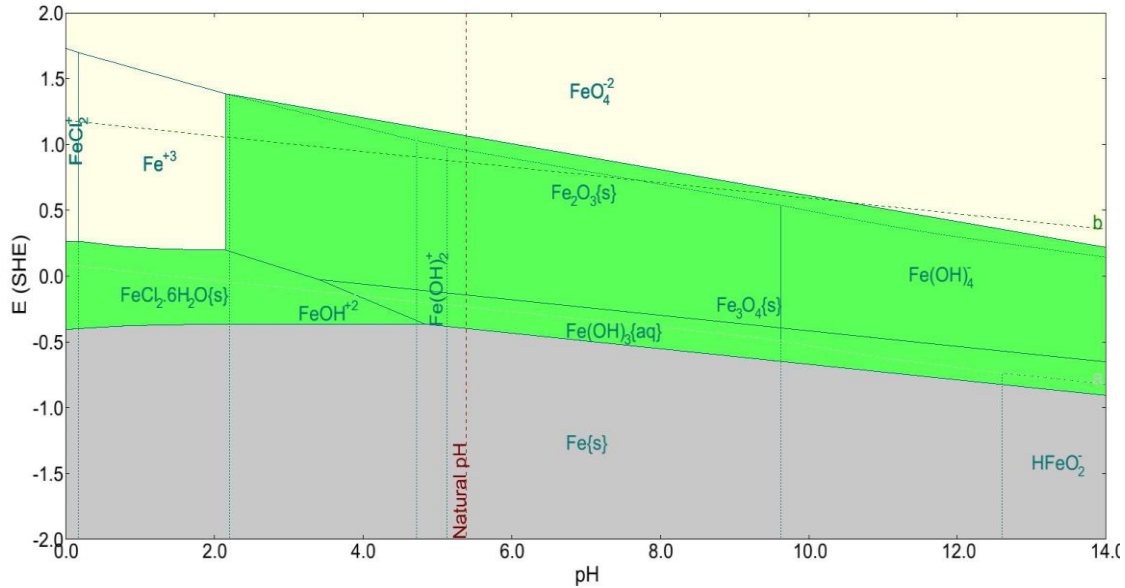


Figure.4.2.1 Pourbaix diagram for steel substrate immersed in a chemical bath.

The Pourbaix diagram is a map for showing the conditions of solution oxidizing power (potential) and acidity or alkalinity (pH) for the various possible phases that are stable in an aqueous electrochemical system. Boundary lines (a and b) on the diagram dividing areas of stability for different phases are derived from the Nernst equation. Potential/pH in some cases is adjusted to prevent corrosion thermodynamically. The Pourbaix diagram shows the reactions and reaction products that will be present when equilibrium has been attained if all appropriate reactions have been included. There are three zones with different colours shown in the Figure 4.2.1. The grey colour represents the immune system of the bath solution from potential (E vs SHE) equal to -2.5V to -0.5V at pH 0 to 14 in which the iron (Fe) metal is formed below the line “a” which is electrolyzed cathodically. The green colour represents the stable region of the bath solution from potential (E vs SHE) equal to -0.5V to 1.75V in which the passive layer is formed from pH 5.0 to 9.5. The yellow colour represents the corrosive system of the bath solution from potential (E vs

SHE) equal to 0.25V to 2.0V in which Fe^{+3} ions are formed from pH 0 to 2 and $\text{Fe}(\text{O}_4)^{-2}$ is formed above line “b” which is electrolyzed anodically to form oxygen gas.

A series of experiments at different parameters was conducted in this study. These parameters are detailed in Table 4.4.

Table 4.2.1 List of the conditions for experimental parameters

<u>Test No.</u>	<u>pH</u>	<u>Temperature °C</u>	<u>Immersion time (Hours)</u>
1	2	40	24
2	2	40	48
3	2	40	72
4	2	50	24
5	2	70	24
6	3	40	24
7	3	40	48
8	3	70	24
9	3	70	48
10	4	80	24
11	4	80	24
12	5	60	24
13	5	80	24
14	5	80	48
15	5	80	72

16	6	50	24
17	6	50	48

For each test, the desired parameters were used to conduct the experiment, the pH of the electrolyte solution was adjusted by drop-wise addition of Hydrochloric acid (HCl), and temperatures were maintained on a laboratory hot plate for the respective immersion times.

Electrochemical measurements were performed using a potentiostat (Ivium Compact Potentiostat) monitoring system connected to a computer for data acquisition and also connected to a three-electrode glass cell set up by applying potential to record the generated readings. The potential range for polarisation resistance technique measurements was from -0.03 V to +0.03 V at a scan rate of 0.125 mV/s.

4.3 SURFACE MORPHOLOGY OBSERVATION AND CORROSION PRODUCT ANALYSIS

After the completion of the electrochemical investigation, samples were taken for morphological and crystal structure characterization. Morphological characterization was done using an FEI MLA 650F Scanning Electron Microscope (SEM) for the high-resolution surface, the Scanning Electron Microscope (SEM) was running at 15 kV, low vacuum mode and images were acquired using a Back-scattered Electron detector (BSED). Bruker Xflash SSD X-ray detectors (EDS) were used for the elementary chemical analysis of the corrosion products. The crystal structure of the corrosion products was characterized by X-ray diffraction (XRD) using a Rigaku Ultima IV X-ray diffractometer with a copper X-ray source (Cu-K- α radiation) operating at 40kV and 44mA and a scintillation counter detector.

5 RESULTS AND DISCUSSION

5.1 EFFECT OF TEMPERATURE ON THE CORROSION BEHAVIOUR OF 13% CHROMIUM STAINLESS STEEL

The polarisation resistance is a useful technique to evaluate and measure the electrochemical behaviour and corrosion rate of stainless steel. It monitors the relationship between electrochemical potential and current generated between electrically charged electrodes in a bath solution to calculate the corrosion rate. The corrosion current density (I_{corr}), corrosion potential (E_{corr}) and anodic and cathodic Tafel slopes (β_a and β_c) were calculated from the intercept on the Tafel slope by the extrapolation process and obtained with reference to saturated silver and silver chloride with potassium chloride as a salt bridge ($\text{Ag}/\text{AgCl}/4\text{MKCl}_{\text{sat}}$) electrode.

The corrosive activity of steel in a corrosive solution is directly related to the corrosion potentials. Structural morphologies, chemical and phase compositions of the samples are directly related to the corrosion resistance of the steel [50]. Below, graphs are the set of experiments showing the corrosion behaviour, corrosion rate and effect of temperature using polarisation technique.

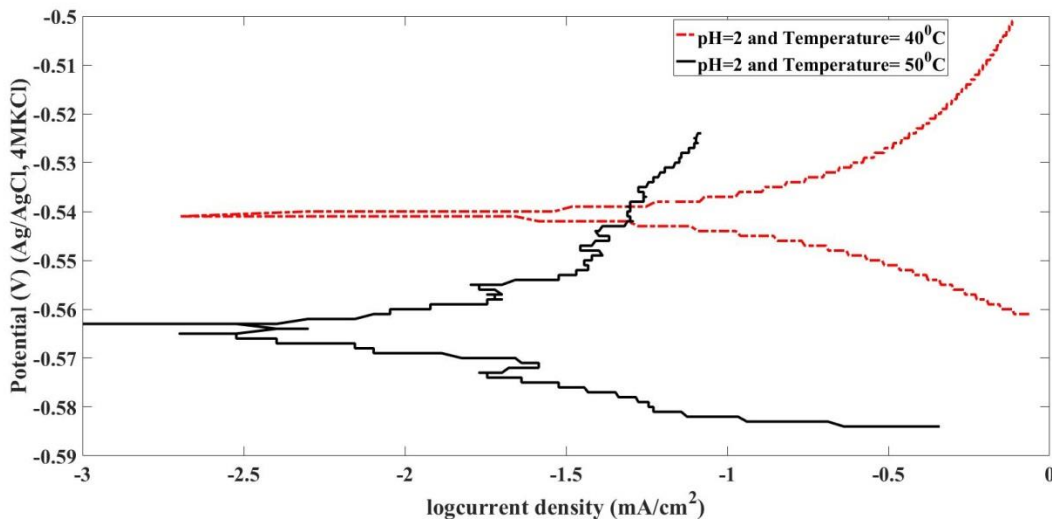


Figure 5.1.1. Polarisation curves of 13% Chromium Stainless steel at different temperatures: 40°C & 50°C at pH2.

The polarisation curves of 13% chromium stainless steel at 40°C and 50°C at pH 2 and an immersion time of 24 hours are shown in Figure 5.1.1. The corrosion current density (I_{corr}) at 50°C is $3.34 \times 10^{-5} \text{ A/cm}^2$ whereas the corrosion current density (I_{corr}) of the sample corroded at 40°C is $1.092 \times 10^{-4} \text{ A/cm}^2$ and there is also a considerable difference in the potential of both parameters. This means that the sample corroded at 50°C possess a lower corrosion current (I_{corr}) value than the sample corroded at 40°C. As is known, the corrosion film formation behaves as a protective barrier, limiting the growth of the corrosion product and preventing the underlying steel from further corrosion [51], [52]. Moreover, an increase in temperature leads to an increase in the corrosion rate, this statement is not satisfied in this case. Figure 5.1.1 shows that the sample at 40°C corrodes more than the sample at 50°C; this is because of the diffusion of species in the chemical solution at 50°C, in the bath solution has a slow rate of film formation compared to the rate of corrosion. Another case for lower temperature to have a higher corrosion rate occurs when the corrosion products have a weak adherence to the steel, causing it to detach and expose the steel surface to the corrosive environment [37].

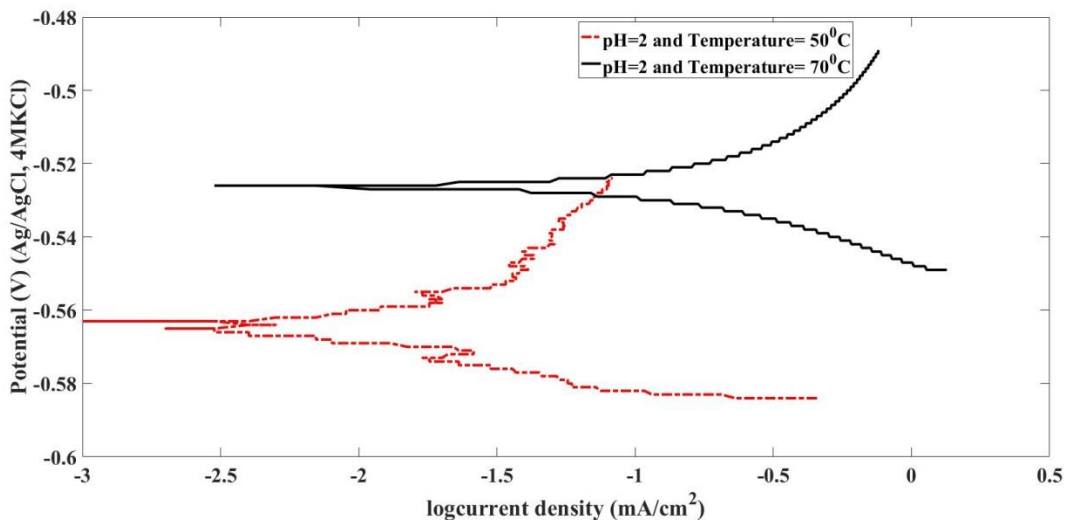


Figure 5.1.2. Polarisation curves of 13% Chromium Stainless steel at different temperatures: 50°C & 70°C at pH2.

In Figure 5.1.2, the polarisation curves of 13% chromium stainless steel at 50°C and 70°C at pH 2 and an immersion time of 24 hours are shown. The corrosion current density (I_{corr}) at 70°C is $5.711 \times 10^{-5} \text{ A/cm}^2$ whereas, the corrosion current density (I_{corr}) of the sample corroded at 50°C is $3.34 \times 10^{-5} \text{ A/cm}^2$. Therefore, the sample corroded at 70°C possesses a higher I_{corr} value than the sample at 50°C. The formation of FeS films acts as a protective barrier, forming faster at a lower temperature and the growth of corrosion product hinders the steel from further corrosion[38]. At a higher temperature, the diffusion of ions takes places more quickly and generates weak passive layer on the metals. Furthermore, there is an increase in the flow of the positive charge from the anodic (oxidation) site toward the cathodic (reduction) site, affecting the dissolution of the steel surface, indicating that the 13% Cr. stainless steel corrodes faster at a higher temperature.

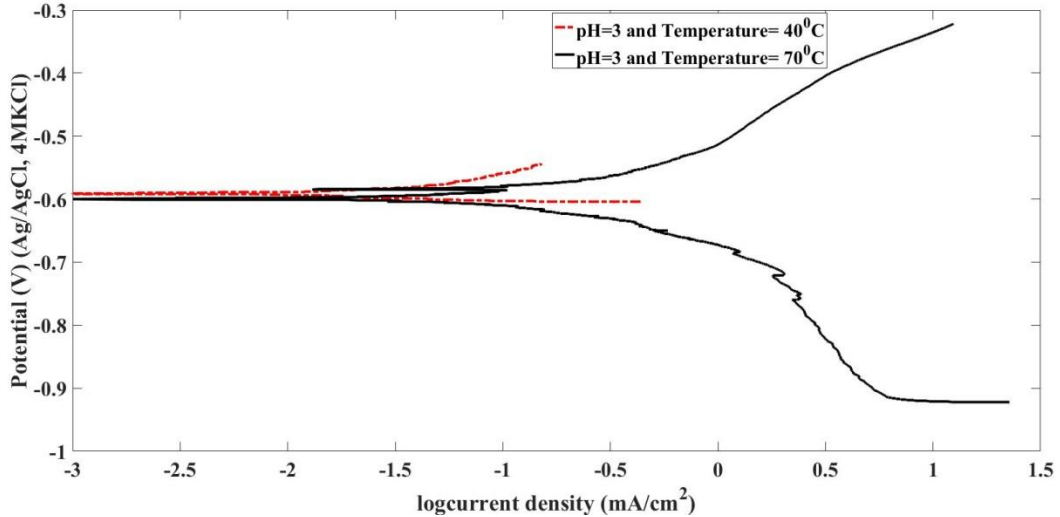


Figure 5.1.3. Polarisation curves of 13% Chromium Stainless steel at different temperatures: 40°C & 70°C at pH3.

In Figure 5.1.3, the polarisation curves of 13% chromium stainless steel at 40°C and 70°C at pH 3 and an immersion time of 24 hours are shown. The corrosion current density (I_{corr}) at 70°C is

$7.048 \times 10^{-5} \text{ A/cm}^2$; however, the corrosion current density of the sample corroded at 40°C is $2.189 \times 10^{-6} \text{ A/cm}^2$. Therefore, the sample corroded at 40°C possess a lower I_{corr} value than the sample at 70°C . The formation of FeS films as the passive layer has an impact on the rate of corrosion, the film forms faster at a lower temperature and the growth of corrosion product limits the steel from further corrosion[38]. At a higher temperature, the chemical reactivity within the corrosive solution increases, which exposes the direct metal surface to the corrosive environment. this also leads to increase in the migration of the charges and the dissolution of the steel surface, implying that the 13% Cr. stainless steel corrodes faster at a high temperature.

5.2 CORROSION RATE WITH RESPECT TO THE CHANGE IN TEMPERATURE

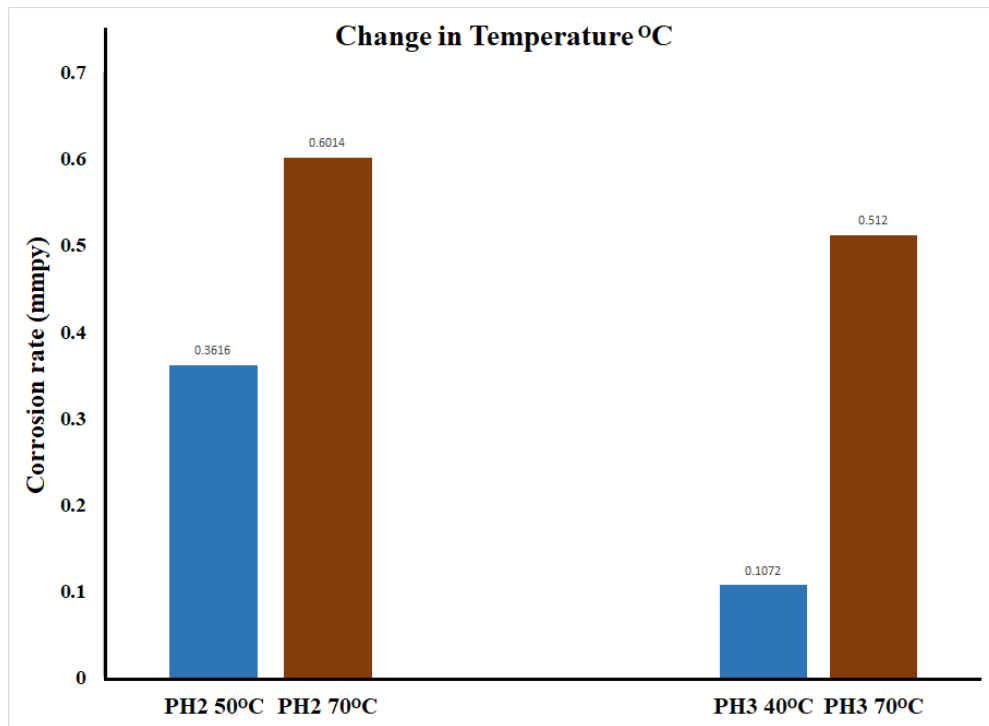


Figure 5.2.1. Corrosion rates measured at different temperatures having the same pH and immersion time.

Figure 5.2.1 shows the corrosion rates at 40°C, 50°C and 70°C with the same immersion time and pH values. An elevated rate of corrosion is observed with the increase in temperature. The corrosion rate recorded by the potentiostat using the polarisation resistance technique at pH2 and 50°C is 0.3616mmpy, whereas the corrosion rate recorded at pH2 and 70°C is 0.6014 mmpy. which occurs due to increased reactivity in the electrolytic solution at a high temperature, causing the polarisation of ions [19].

5.3 EFFECT OF PH VALUE ON THE CORROSION BEHAVIOUR OF 13% CHROMIUM STAINLESS STEEL

The graphs below are the set of experiments showing the corrosion behaviour, corrosion rate and the effect of pH.

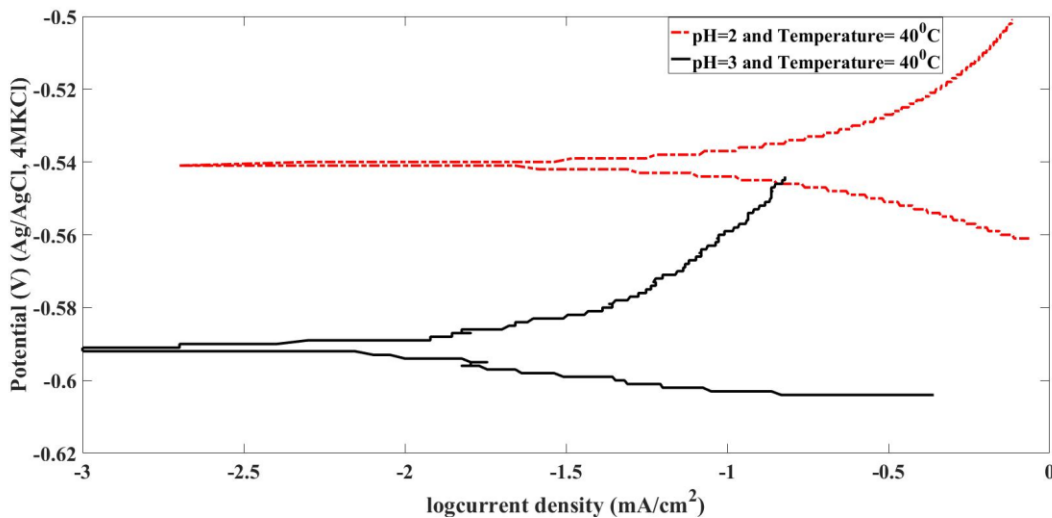


Figure 5.3.1 Polarisation curves of 13% Chromium Stainless steel at different pH: 2 and 3 at 40°C.

The pH value of the solution has an enormous impact on the composition of the corrosion products and their passive nature. At a lower pH, the solubility of the solution is very high, which makes

the precipitation of iron sulphide (FeS) difficult on the steel surfaces [53]. Due to this, the passive layer formation is minimal or weak, which increases the corrosion rate. This can also be explained by the increased corrosion current density (I_{corr}). Figure 5.3.1 shows the polarisation curves of 13% chromium stainless steel at pH 2 and pH 3 at 40°C and an immersion time of 24 hours. A lower pH 2 value has a corrosion current density (I_{corr}) of $1.092 \times 10^{-4} \text{ A/cm}^2$, whereas the corrosion current density (I_{corr}) of the sample at higher pH 3 is $2.189 \times 10^{-6} \text{ A/cm}^2$. Therefore, the sample at pH 2 corrodes more than the sample at pH 3.

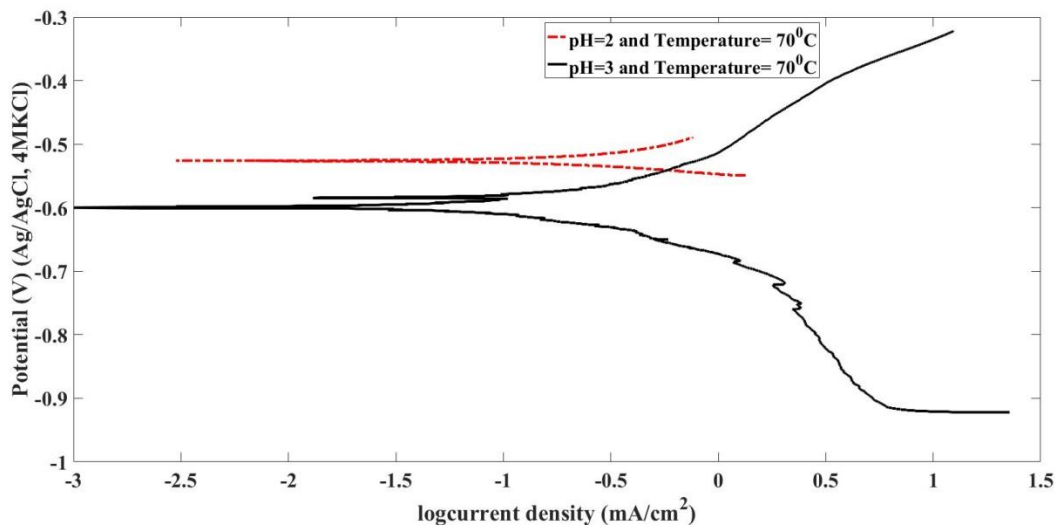


Figure 5.3.2. Polarisation curves of 13% Chromium Stainless steel at different pH: 2 and 3 at 70°C.

In the experimental case above, a significantly higher temperature was used. The electrolytic solution was set at the parameters of 70°C, pH 2, 3 and an immersion time of 24 hours. This particular experimental case shows the correlation between pH value and the corrosion rate. In Figure 5.3.2, the corrosion current density (I_{corr}) at pH 2 is $5.711 \times 10^{-5} \text{ A/cm}^2$, whereas the corrosion current density (I_{corr}) at pH 3 is 7.048×10^{-5} , which means that the particular case of the

sample at pH 3 is more corroded than the sample at pH 2 and 70°C. This indicates that at pH 3, the dissolution of chemical species in the solution has formed a fragile passive layer which has easily detached from the steel surface, exposing the underlying steel in the highly corrosive environment [52], [54].

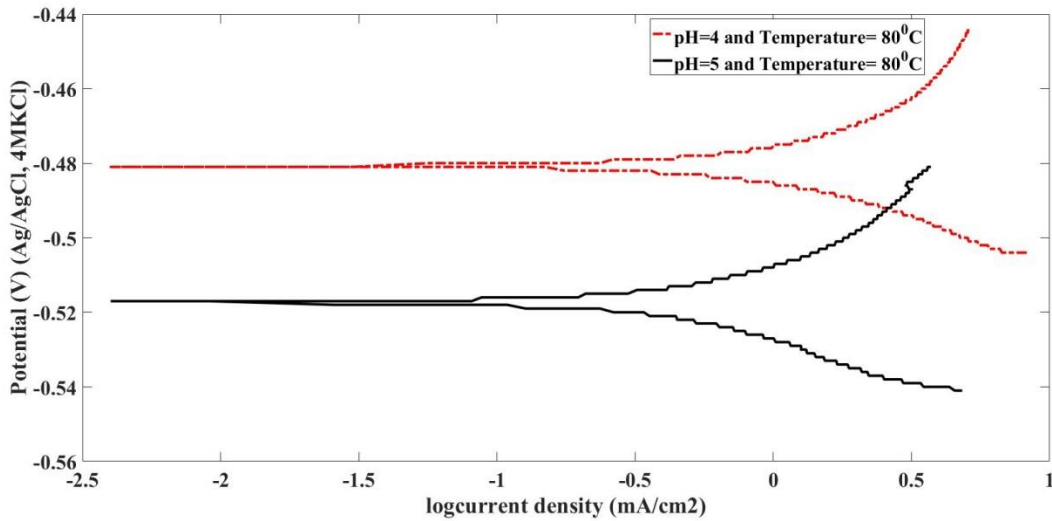


Figure 5.3.3. Polarisation curves of 13% Chromium Stainless steel at different pH: 4 and 5 at 80°C.

In above case, the experimental comparison is between pH 4 and pH 5. The parameters are a temperature of 80°C, pH of 4, 5 and immersion time of 24 hours. The corrosion current density (I_{corr}) recorded at pH 4 is $7.431 \times 10^{-4} \text{ A/cm}^2$ and the corrosion current density (I_{corr}) at pH 5 is $3.543 \times 10^{-4} \text{ A/cm}^2$. This demonstrates that the corrosion rate of the steel sample at pH 4 is higher than for the sample at pH 5. The inhibitive effect due to the formation of iron sulphide layers occurs mostly between pH 3 to pH 5 [14] which explains the corrosion behaviour more precisely at these pH values.

5.4 CORROSION RATE WITH RESPECT TO THE CHANGE IN PH VALUE

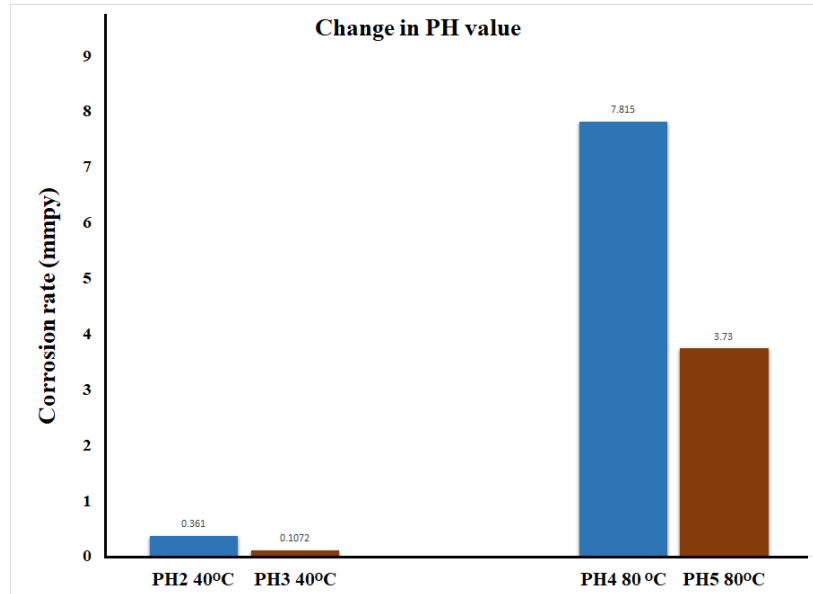


Figure 5.4.1. Corrosion rates measured at different pH values having the same temperature, immersion time.

Figure 5.4.1 shows the corrosion rates calculated at different pH values, i.e. pH2, pH3, pH4, pH5 with the same temperature. The corrosion rate decreases with the increase in pH value. The corrosion rate recorded by the potentiostat using the polarisation resistance technique at pH2 and 40°C is 0.361mmpy, whereas the corrosion rate recorded at pH3 40°C is 0.1072mmpy. The past research reports that when the pH value is decreased, the corrosive film becomes de-passivated, which results in an unprotected steel surface [55],[51],[56],[57] in the H₂S environment, which rapidly changes the corrosion reactivity, as seen in Figure 5.4.1.

5.5 EFFECT OF IMMERSION TIME ON THE CORROSION BEHAVIOUR OF 13% CHROMIUM STAINLESS STEEL

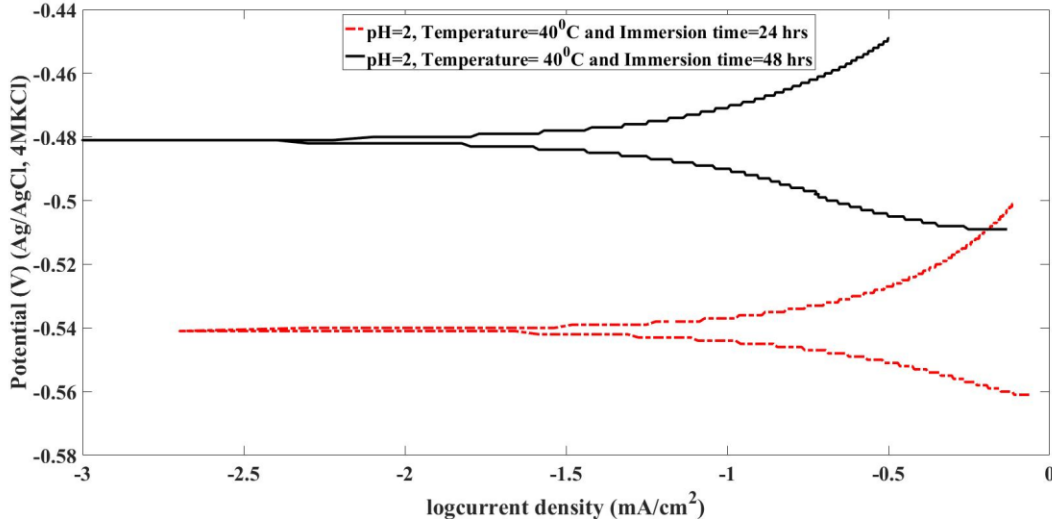


Figure 5.5.1. Polarisation curves of 13% Chromium Stainless steel at different immersion times: 24 hours and 48 hours at pH2, 40°C.

In this case, the experimental parameters are at a temperature of 40°C and pH 2 with a change in the immersion time from 0 to 24 hours and 24 to 48 hours. Figure 5.5.1 shows that the corrosion rate of an immersion time of 24 hours is slightly higher than the rate at 48 hours. The corrosion current density (I_{corr}) is $1.092 \times 10^{-4} \text{ A/cm}^2$ at 24 hours, which is lower than the corrosion current density (I_{corr}) of $3.339 \times 10^{-5} \text{ A/cm}^2$ at 48 hours.

The Figure 5.5.2 shows the results for experimental parameters of a temperature 40°C and pH 3 with a change in immersion time from 0 to 24 hours and 24 to 48 hours. Figure 5.5.2 shows the analysis of the effect of immersion time with an increase in pH value. The corrosion rates are different for both immersion times, which can be explained by the weakly formed passive layer [58].

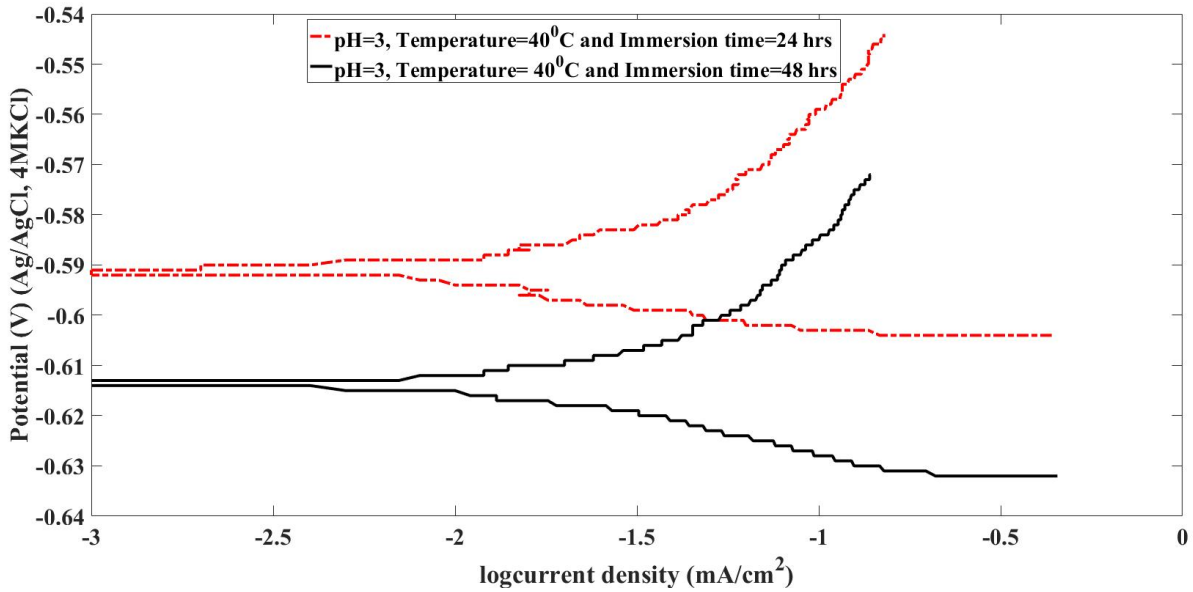


Figure 5.5.2. Polarisation curves of 13% Chromium Stainless steel at different immersion times: 24 hours and 48 hours at pH3, 40°C.

As the immersion time increases, the weak, passive layer starts to break, due to fast chemical reactions. This results in the longer immersion time having a higher corrosion rate than the experiment with a shorter immersion time.

The corrosion current density (I_{corr}) for an immersion time of 24 hours is $2.189 \times 10^{-6} \text{ A/cm}^2$. However, the corrosion current density (I_{corr}) at 48 hours is $1.1018 \times 10^{-5} \text{ A/cm}^2$. This means that the corrosion rate of the sample at the immersion time of 24 hours is higher compared to the corroded sample at 48 hours when the pH is increased.

In this particular case, the impact of the pH value can be seen as the immersion time changes.

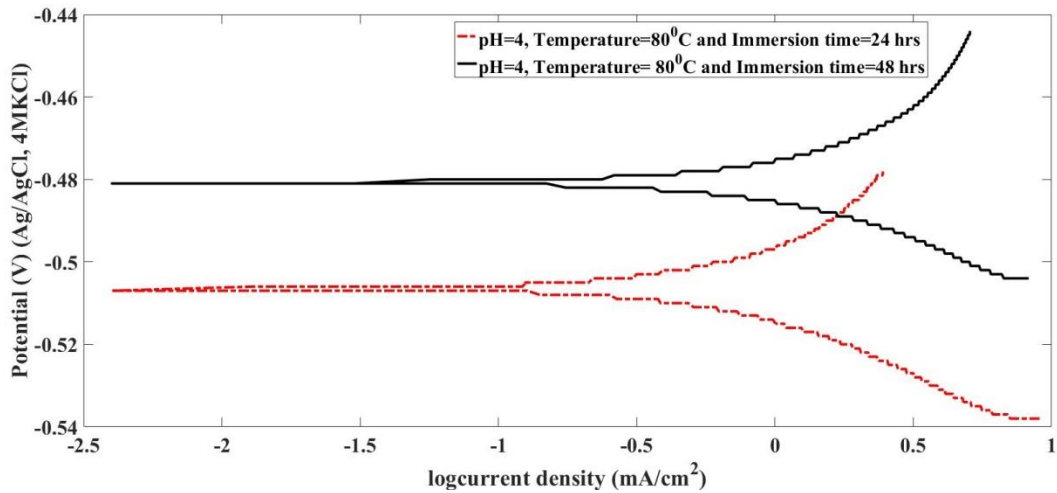


Figure 5.5.3. Polarisation curves of 13% Chromium Stainless steel at different immersion times: 24 hours and 48 hours at pH3, 80°C.

The parameters used in the experiment above are a temperature of 80°C and pH 3 with a change in the immersion time from 0 to 24 hours and 24 to 48 hours. Figure 5.5.3 shows the corrosion rate for both immersion times has a slight difference despite the increase in temperature. This can be explained by the breaking of the passive FeS layer. The passive layer starts to break with an increased chemical reaction as time increases [36]. This results in the immersion time of 48 hours having a higher corrosion rate compared to the experiment at an immersion time of 24 hours. The corrosion current density (I_{corr}) for the immersion time of 24 hours is $7.431 \times 10^{-4} \text{ A/cm}^2$, whereas the corrosion current density (I_{corr}) at 48 hours is $8.514 \times 10^{-4} \text{ A/cm}^2$. This means the corrosion rate of the sample at an immersion time of 48 hours is higher, compared to the corroded sample at 24 hours, when the temperature is increased. In this particular case, the effect of temperature can also be seen along with the change of immersion time.

5.6 CORROSION RATE WITH RESPECT TO THE CHANGE IN IMMERSION TIME

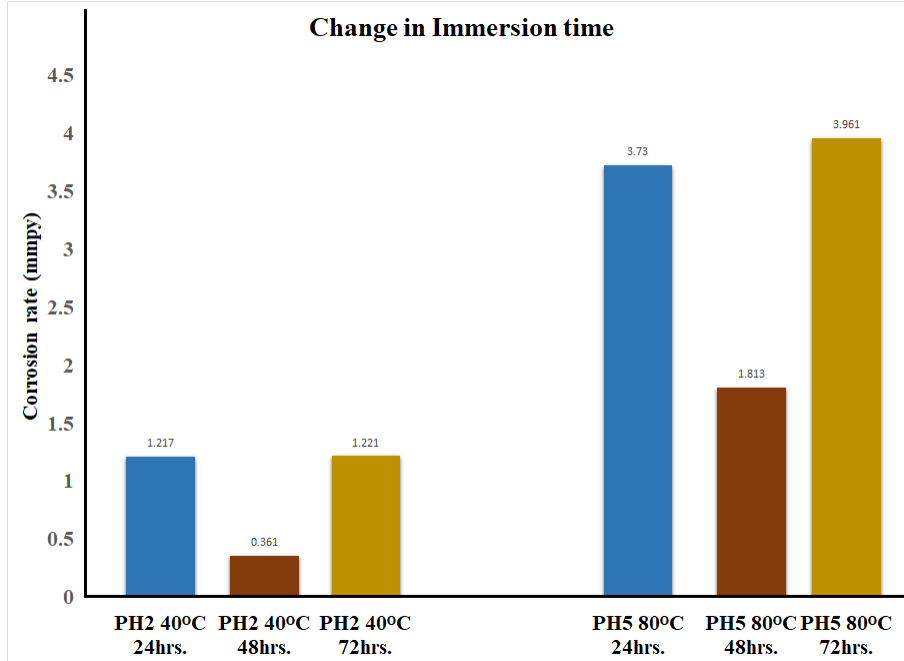


Figure 5.6.1. Corrosion rates measured at different immersion times having the same temperature and pH value.

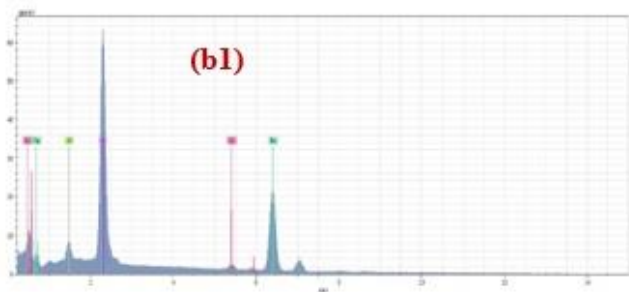
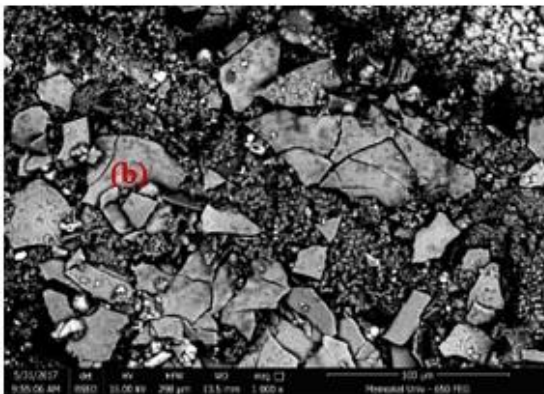
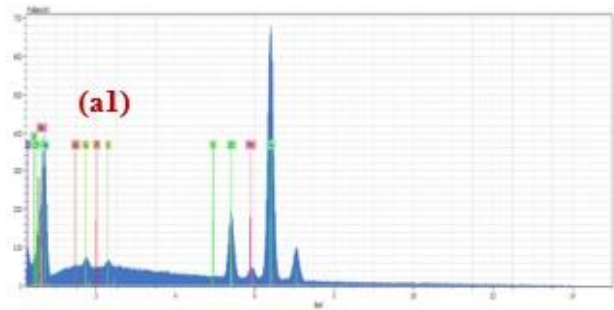
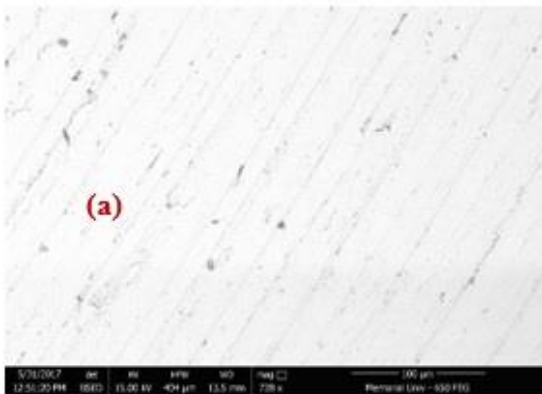
Figure 5.6.1 shows the corrosion rates calculated at the different immersion times of 24hours, 48hours and 72hours with the same pH values and temperatures. The corrosion rate changes significantly with an increase in immersion time. The corrosion rate recorded by the potentiostat using polarisation resistance method at 24hours of immersion time and pH2 at 40°C is 1.217 mmpy, and then it is observed that the corrosion rate is decreased at 48hours, pH2 and 40°C, resulting in corrosion rate of 0.361mmpy. The corrosion rate is observed to increase again to 1.221 mmpy with further increase in immersion time of 72hours, pH2 and 40°C. When the steel sample is first immersed in the electrolytic solution, the steel surface starts reacting chemically to the solution, causing it to corrode and with an initial increase in immersion time, the passive layer

begins to form on the steel surface. The passive layer acts as a barrier between the steel and electrolytic solution, resulting in a decrease in corrosion rate, but when the immersion time is further increased, the passive layer starts depassivating, due to which the corrosion rate increases even more, as seen in Figure 5.6.1[59].

5.7 SCANNING ELECTRON MICROSCOPE (SEM) AND ENERGY DISPERSIVE X-RAY SPECTROSCOPY (EDS)

The SEM analysis was conducted to study the morphological characterization of the corrosion products in different H₂S environmental conditions. Figure 5.7.1(a) shows the SEM image of an original uncorroded sample. EDS analysis has determined the composition of the substrate, which matches the chemical composition of steel reported in Table 4.2.

S.N. Smith (2002) reported that the sequential resistance of corrosion products, mainly FeS, formed in the H₂S environment are as follows: Mackinawite < Troilite < Pyrrhotite < Pyrite [60].



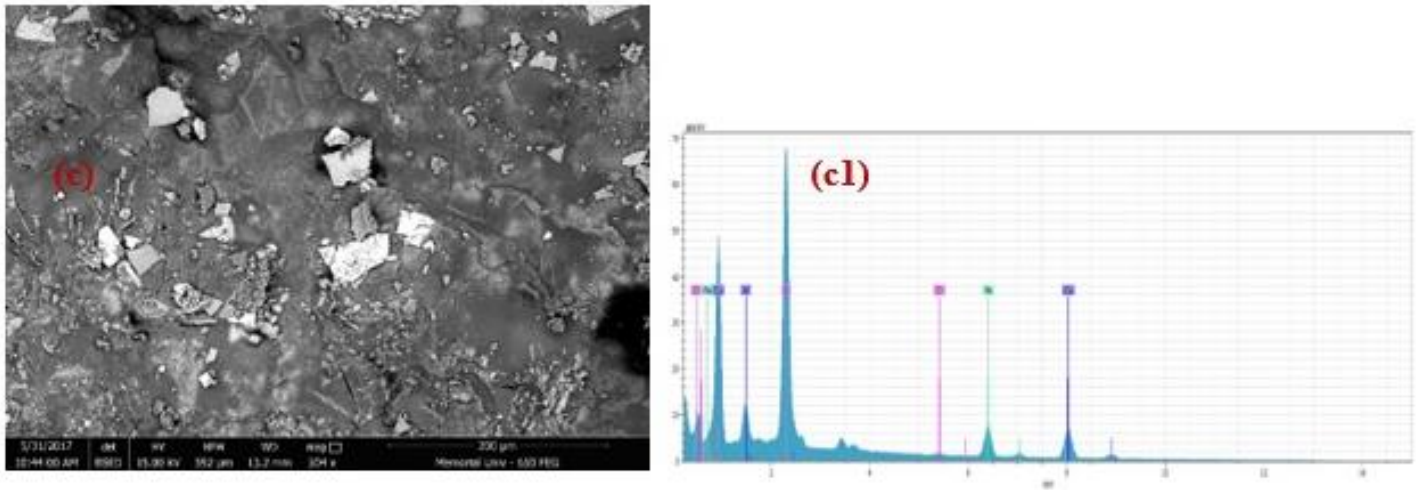


Figure 5.7.1 SEM images and EDS analysis of the corrosion products formed on the steel surface for (a) Original uncorroded sample. (b) pH 2, 50°C, 24 hours. (c) pH 2, 70°C, 24 hours.

The corroded sample at pH 2, 50°C and 24 hours is shown in Figure 5.7.1(b). The magnified SEM image shows the layer of pyrite and iron sulphide (FeS) films on the steel surface. The thick corrosion layer observed in the SEM image is cracked, due to the diffusion of the electrochemical reaction at a high temperature[61]. The EDS analysis in Figure 5.7.1 (b1) shows that a high amount of sulphur has lead to the formation of a thick corrosion layer.

In Figure 5.7.1(c) the sample was corroded at a higher temperature of 70°C at pH 2 for 24 hours. The SEM images show the loose and rough formation of corrosion film due to the increased reactivity in the chemical bath at a significantly high temperature and lower pH. The EDS analysis in Figure 5.7.1(c1) shows a higher amount of sulphur.

Comparing Figure 5.7.1(b) at 50°C and Figure 5.7.1(c) at 70°C, it can be seen from Figure 5.7.1(c) that the changes in temperature in the chemical reaction affect corrosion film formation. Both SEM images demonstrate that a higher temperature prevents the creation of the passive layer, due to the high reactivity in the electrochemical bath.

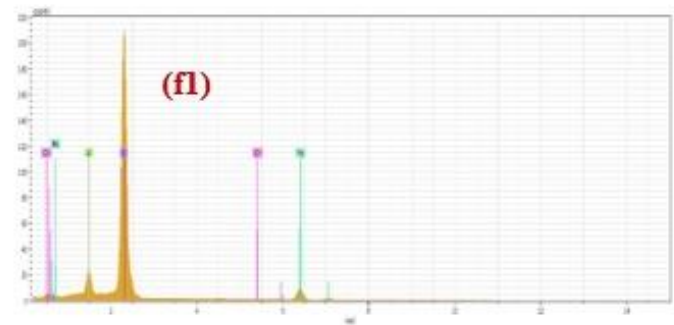
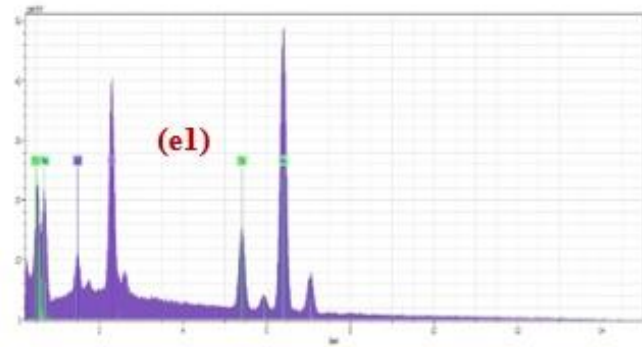
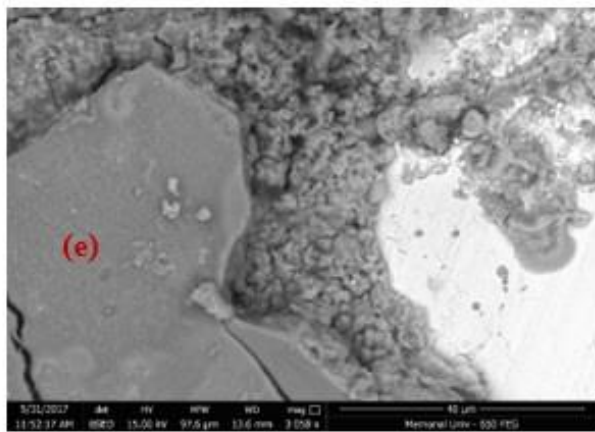
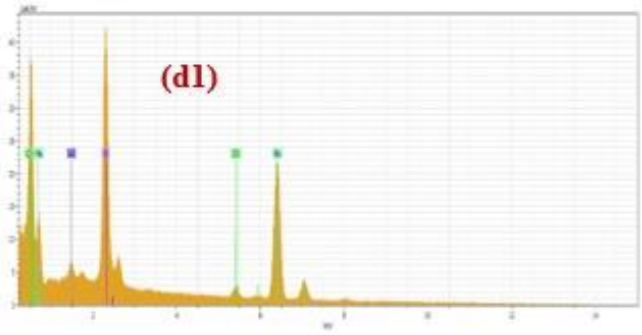
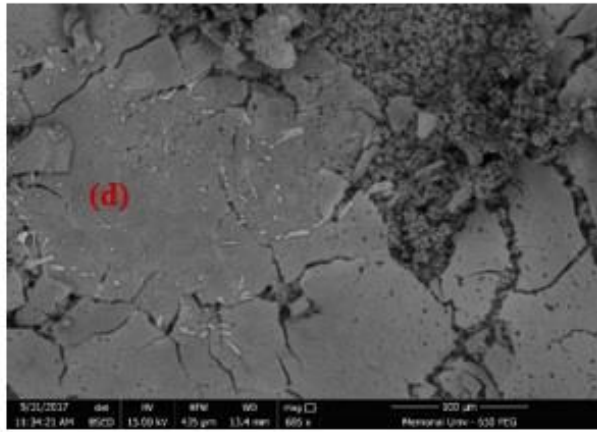


Figure 5.7.2 SEM images and EDS analysis of the corrosion products formed on the steel surface for (d) pH 3, 40°C, 48 hours. (e) pH 3, 70°C, 48 hours. (f) pH 4, 80°C, 48 hours.

Figure 5.7.2(d) shows the SEM image of a corroded sample at pH 3, 40°C and 48 hours. In the scanning electron microscope (SEM) image it can be seen that the steel surface is consistently covered with a thick corrosion layer, which is also called corrosion protective film. EDS analysis records the least amount of sulphur contents in the corrosion layer. As explained previously, at a lower temperature and higher pH the corrosion sample is easily passivated, which prevents the steel from further corrosion [62].

In this sample, the temperature is increased from 40°C to 70°C. The corroded sample at pH 3, 70°C and 48 hours shown in Figure 5.7.2(e), the magnified SEM image shows the breaking of the thick corrosion layer along with the loose blister of the corrosion layer on the right side of the image. Although there is a high volume of the precipitated corrosion layer on the surface, the increase in temperature starts peeling off the deposited layer, exposing the steel to the harsh environment, which quickly accelerates the corrosion rate [63]. The EDS analysis in figure 5.7.2 (e1) shows high amounts of sulphur and iron contents.

In Figure 5.7.2(f) the sample is corroded at a temperature of 80°C at pH 4, 48 hours. The SEM images show a fragile layer of corrosion film, due to the increased reactivity in the chemical bath due to the change in temperature. The EDS analysis shown in figure 5.7.2(f1) confirms higher amounts of sulphur.

Comparing Figure 5.7.2(d) at 40°C and Figure 5.7.1(e) at 70°C, it can be seen from figure 5.7.1(e) that the temperature influences the rate of the chemical reaction and its effect on the formation of corrosion film. Both SEM images demonstrate that the corrosion layers are loosely packed at a higher temperature with a rough distribution on the steel surface.

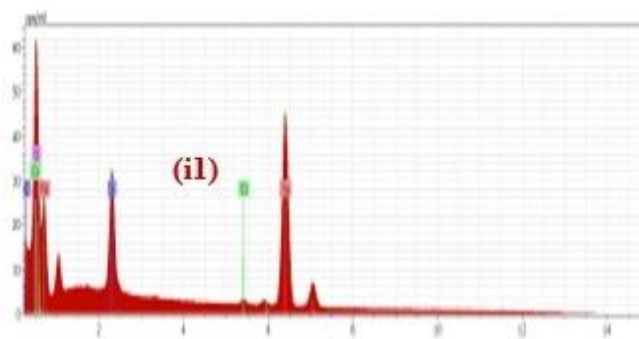
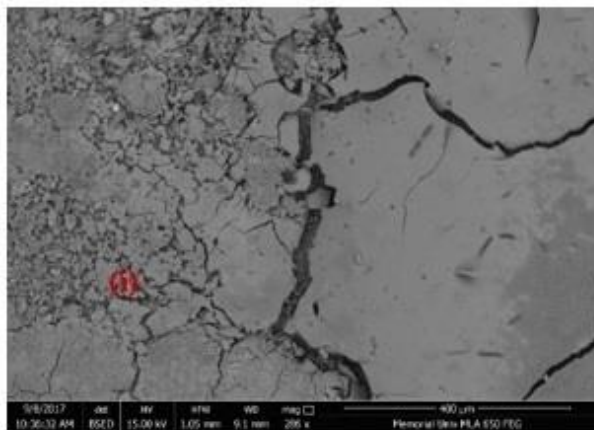
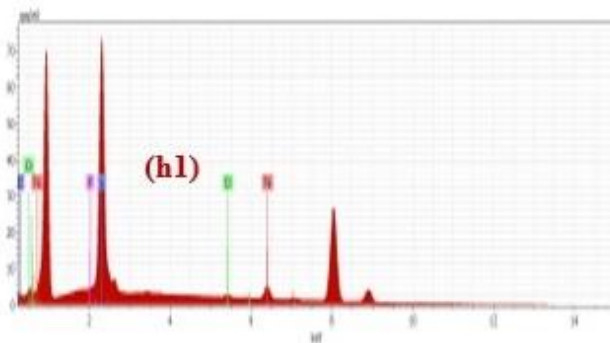
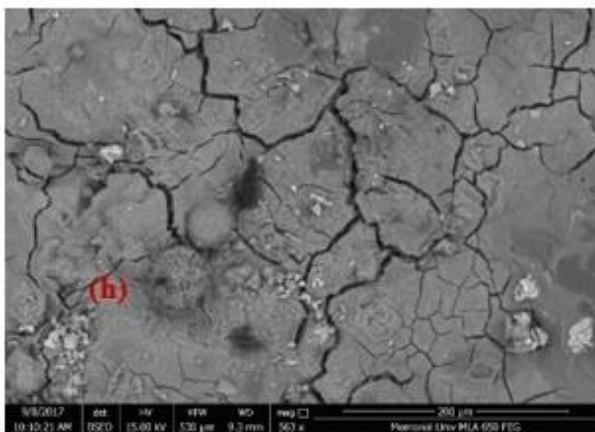
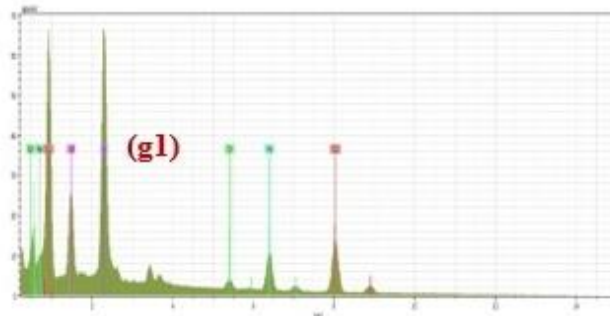


Figure 5.7.3 SEM images and EDS analysis of the corrosion products formed on the steel surface for (g) pH 5, 80°C, 48 hours. (h) pH 6, 50°C, 24 hours. (i) pH 6, 50°C, 48 hours.

Figure 5.7.3(g) shows the SEM image of a corroded sample at pH 5, 80°C and 48 hours. The SEM image shows a high volume of precipitation of the corrosion layer on the steel surface.

As the pH values increase, the corrosion product becomes insoluble in the chemical bath, which also increases the rate of precipitation on the passive layer observed on the steel surface, which limits the corrosion reactivity [36]. Therefore, in Figure 5.7.3(g1) the EDS analysis shows a significant amount of sulphur content in the corrosion layer.

In this sample, the pH value is increased from pH 5 to pH6 with a decrease in temperature. The corroded sample at pH 6, 50°C and 24 hours is shown in Figure 5.7.3(h). The magnified SEM image shows a well-formed corrosion layer with higher precipitation; this is due to a high pH value and lowered temperature, which increases the precipitation of the corrosion product on the steel surface and limits the reaction between the electrolytic solution and the corrosion product. The EDS analysis in Figure 5.7.3 (h1) shows a large amount of sulphur and iron precipitation on the sample surface.

In this sample, the immersion time is increased from 24 hours to 48 hours. Figure 5.7.3(i) shows the sample corroded at a temperature of 50°C at pH 6 and 48 hours. The SEM image shows that a thick layer of corrosion film has formed on the surface. Increase in immersion time decreases the chemical reactivity between the corrosive film and the chemical bath. It allows further precipitation and formation of the passive layer. The EDS analysis is shown in Figure 5.7.3(i1) shows the chemical composition of the corrosion products, which have a significant amount of sulphur and iron.

Comparing between Figure 5.7.3(g), Figure 5.7.3(h) and Figure 5.7.3(i), it is observed that when there is an increase in pH value or an increase in the immersion time, the volume of precipitation of the corrosion product on the steel surface also increases, forming a thick corrosion layer.

5.8 X-RAY DIFFRACTION (XRD)

The corrosion products formed on the steel surface are characterized using X-ray diffraction (XRD). The crystal phase characterization of the corrosion products identifies the peaks. Different databases are used, such as Powdered diffraction files (PDF), RDB Minerals and the International Centre for Diffraction database (ICDD).

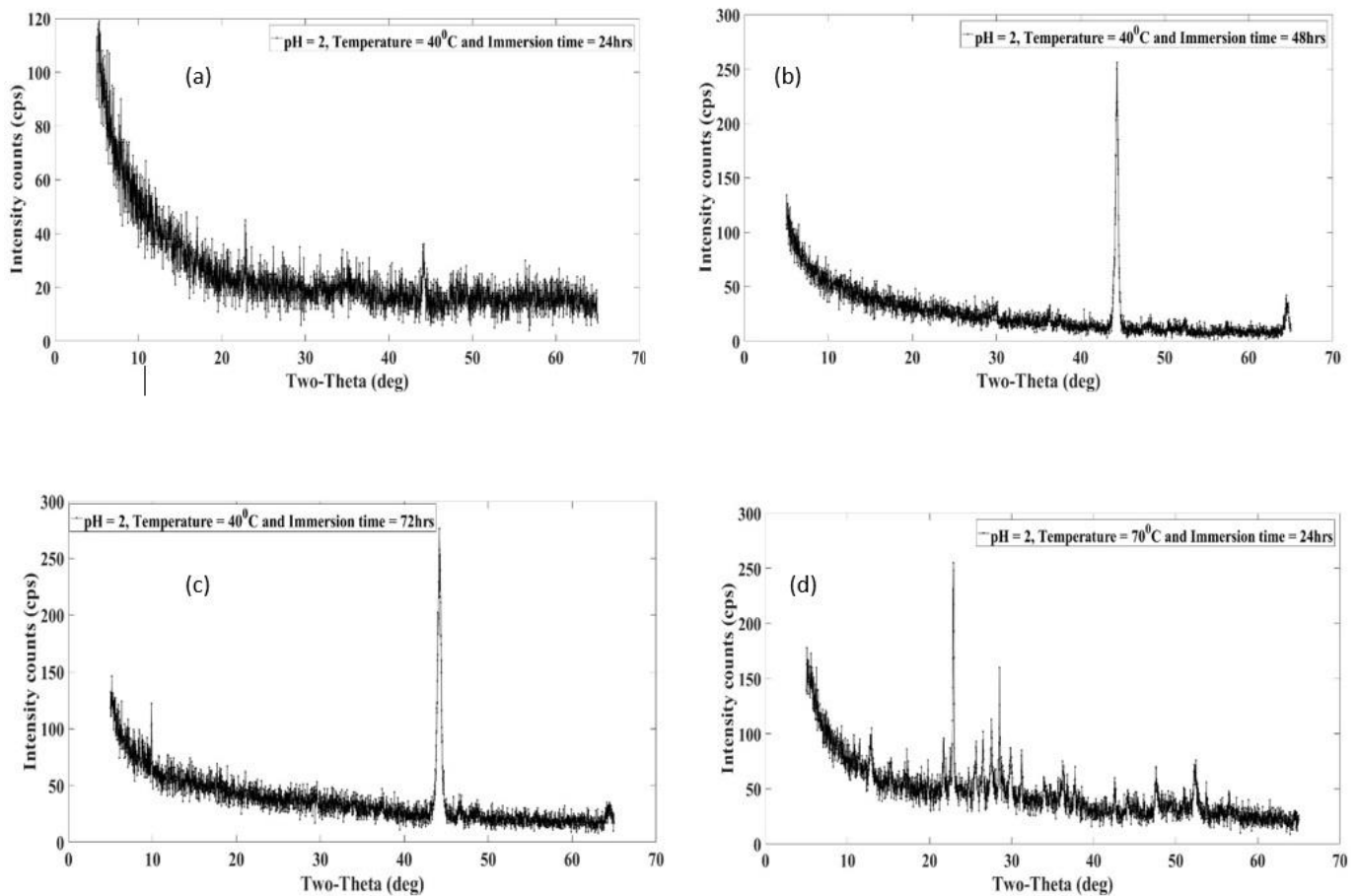


Figure 5.8.1. XRD analysis of the corrosion product formed on the steel surface at: (a) 40°C, pH2 and 24 hours, (b) 40°C, pH2 and 48 hours, (c) 40°C, pH2 and 72 hours, (d) 70°C, pH2 and 24 hours.

In Figure 5.8.1(a) the peaks are matched by the PDF #[00-006-0696]. Identifying the iron (Fe) as a body centred cubic (BCC) structure, XRD peaks in the figure 5.8.1(b) match the PDF # [00-016-0713] identifying the corrosion product as Greigite (Fe_3S_4) with a cubic crystal structure; this suggests that the corroded sample after an increase in the immersion time, formed a corrosion product on the steel surface. In Figure 5.8.1(c) the peaks are identified as iron (Fe) [00-006-0696] as the cubic crystal structure, pyrite (FeS_2) [00-042-1340] as the cubic structure and iron sulphide (FeS) [0-065-1984] as the orthorhombic crystal structure.

In Figure 5.8.1(d), the corrosion products formed on the steel surface are identified as iron sulphide (FeS) [98-001-1763], iron (Fe) [00-006-0696] and pyrite (FeS_2) [98-002-0637]. These corrosion products are minerals of iron sulphide (FeS) which have been precipitated on the steel surface in various H_2S environmental parameters [3], [60].

In Figure 5.8.2(e), the XRD characterization has identified the peaks of corrosive product film on the steel surface as iron (Fe) [00-006-0696] with a cubic crystal structure and pyrrhotite (Fe_7S_8) [98-000-1338] with a monoclinic crystal system.

Figure 5.8.2(f) has a database-matched finding of the corrosion products as iron (Fe) [98-001-7162] and greigite (Fe_3S_4) [98-00-1180]. Both minerals are formed as cubic crystal structures along with a less amount of iron sulphide (FeS) [98-001-1762].

However, in Figure 5.8.2(g), the deposited corrosive products are pyrite (FeS_2) [98-002-0637] and iron (Fe) [98-001-9692] and also in Figure 5.8.2(h) iron sulphide and pyrite formed on the steel substrate is also known as fool's gold (FeS_2) [00-0042-1340].

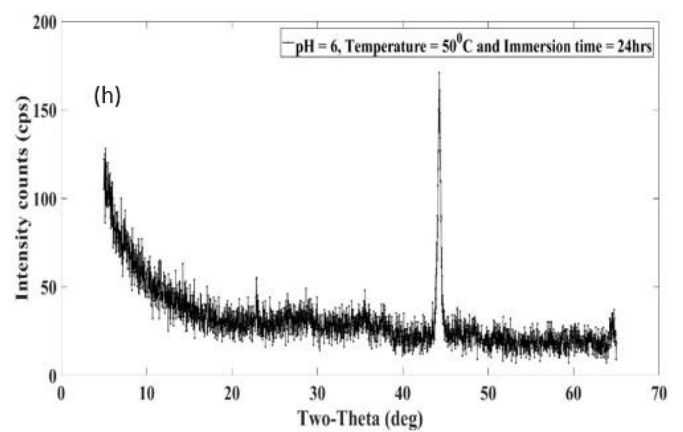
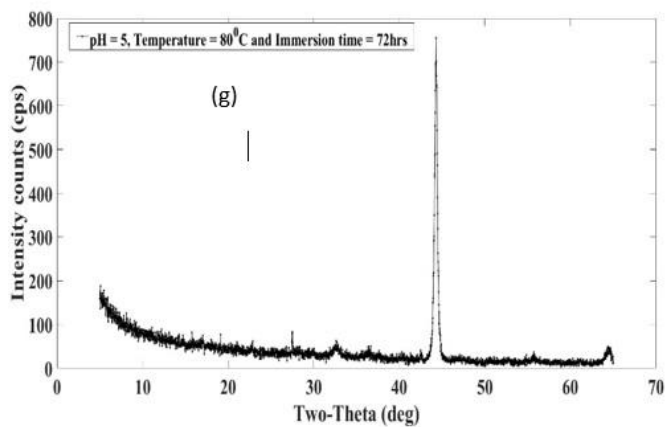
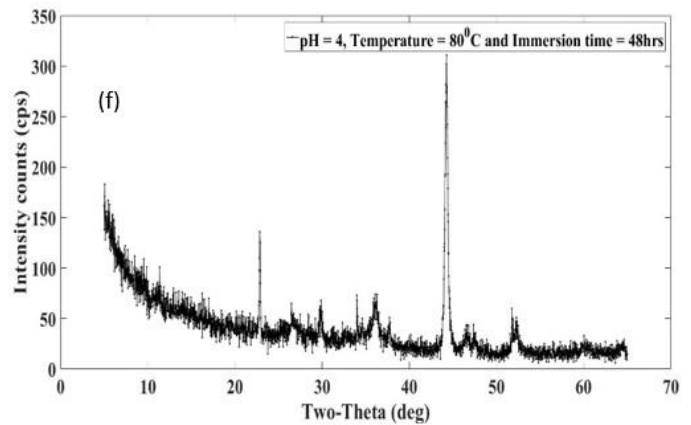
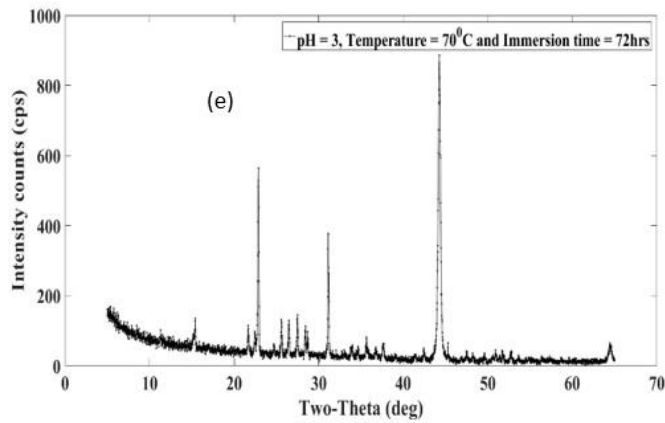


Figure 5.8.2. XRD analysis of the corrosion product formed on the steel surface at: (e) 70°C, pH3 and 72 hours, (f) 80°C, pH4 and 48 hours, (g) 80°C, pH5 and 72 hours, (h) 50°C, pH6 and 24 hours.

This characterization demonstrates that the change in parameters such as temperature, pH and immersion time has a significant impact on the corrosion behaviour. The mechanism of passive layer formation results in the growth of different FeS minerals.

6 CONCLUSION

The results of this work are important findings with respect to the corrosion behaviour in sour environments.

- In an H₂S environment, the corrosion rate increases with the increase in temperature but after 70°C the effect of temperature lessens.
- The corrosion rates decrease with an increase in the pH value and the pH of the environment has a huge impact on the corrosion rate and the formation of protective films on the steel surface.
- For a short period of time the corrosion rates decrease with an increase in immersion time, but over an extended period the protective layer becomes weak and starts to corrode the steel beneath the protective film
- The formation of a film on a steel surface is dependent on the pH and temperature of the environment. Lower temperature and higher pH form thick and uniform protective films which eventually decrease the corrosion rate and protect the steel from exposure to the corrosive media.
- Different types of oxides formed on the surface have different effects on the corrosive resistivity of the steel and the formation of stable oxides lowers the rate of corrosion.

7 FUTURE WORK AND RECOMMENDATIONS

This thesis has many limitations due to the safety concerns associated with the H₂S gas and the lab's suitability.

- Further research is needed to enhance the findings using H₂S gas with better provisions for safety.
- The concentration of H₂S should also be considered for the development of this research.
- Corrosion behaviour at a very high temperature is still unclear, and more research is needed for better understanding of corrosion behaviour with elevated temperatures.
- The experimental time in this thesis is a maximum of 72 hours, which could be increased in future research work.
- Study of each FeS oxide is needed to study the growth mechanism of protective films.

REFERENCES

- [1] J. Fritz and D. H. Russ, "H₂S Multiphase Flow Loop: CO₂ Corrosion in the Presence of Trace Amounts of Hydrogen Sulfide," *Eng. Technol.*, November, 2004.
- [2] W. Yan, P. Zhu, and J. Deng, "Corrosion behaviors of SMSS 13Cr and DSS 22Cr in H₂S/CO₂-oil-water environment," *Int. J. Electrochem. Sci.*, vol. 11, no. 11, pp. 9542–9558, 2016.
- [3] A. F. Goncharov *et al.*, "Hydrogen sulfide at high pressure: Change in stoichiometry," *Phys. Rev. B*, vol. 93, no. 17, p. 174105, 2016.
- [4] G. Xian Zhao, X. Hong Lu, J. Min Xiang, and Y. Han, "Formation Characteristic of CO₂ Corrosion Product Layer of P110 Steel Investigated by SEM and Electrochemical Techniques," *J. Iron Steel Res. Int.*, vol. 16, no. 4, pp. 89–94, 2009.
- [5] S.D. Kapusta, B.F.M. Pots and R.A. Connell, "Corrosion Management of Wet Gas Pipelines," in *Proc. Corrosion*, 1999.
- [6] R. Heidersbach, "Metallurgy and Corrosion Control in Oil and Gas Production.," *John Wiley and Sons*, 2011.
- [7] L. R. Faulkner, A. J. Bard, "Electrochemical Methods: Fundamentals and Applications," *John Wiley and Sons*, Edition 2, pp. 24–25, 2001.
- [8] Gabriel N. Meloni, "Building a Microcontroller Based Potentiostat: an Inexpensive and Versatile Platform for Teaching Electrochemistry and Instrumentation," pp. 1320–1322, 2016.
- [9] M. Vergani, "Electronic Instrumentation for Electrochemical Cell Monitoring in Lab-on-

- Chip Devices,” 2012.
- [10] M. A. P. Henry Fu, Henry Chow, Michael Lew, Shruti Menon and Craig Scratchley, “An Electrochemical Potentiostat Interface for Mobile Devices: Enabling Remote Medical Diagnostics,” pp. 1–5, 2015.
- [11] Autolab Application Note EC08, “Basic overview of the working principle of a potentiostat/galvanostat (PGSTAT) – Electrochemical cell setup,” *Metrohm Autolab.B.V*, pp. 1–3, 2011.
- [12] D. McMullan, “Scanning Electron Microscopy,” in *51st Annual Meeting of the Microscopy Society of America*, 1965.
- [13] Haitao Fang, "Investigation of Localized Corrosion of Carbon Steel in H₂S Environments," Ph.D. Thesis, Russ College of Engineering and Technology of Ohio University, March, 2012.
- [14] B. Valery, “Effect of Pre-exposure of Sulfur and Iron Sulfide on H₂S Corrosion at Different Temperatures,” pp. 1–68, Master's Thesis, University of Stavanger, June, 2011.
- [15] Y. Zheng, “Electrochemical Mechanism and Model of H₂S Corrosion in Carbon steels,” Ph.D. Thesis, Russ College of Engineering and Technology of Ohio University, May, 2015.
- [16] H. Fang, D. Young, and S. Nešić, “Elemental Sulfur Corrosion of Mild Steel At High Concentrations of Sodium Chloride,” *NACE Int.*, Paper No. 2592, pp. 1–16, 2009.
- [17] N. Yaakob, “Top of the Line Corrosion in CO₂/H₂S Environments,” pp. 1–198, Ph.D. Thesis, Russ College of Engineering and Technology of Ohio University, May, 2015.
- [18] A. Narasimhavarman, “Engaging Degradation Mechanisms Of Materials In A Tourney. An

- Investigation Into The Philosophy Of Material Selection As A Mitigating Measure and Strategy,” Master's Thesis, University of Stavanger 2013.
- [19] H. Taheri, S. Kakooei, M. C. Ismail, and A. Dolati, “The Effect of H₂S Concentration and Temperature on Corrosion Behavior of Pipeline Steel A516-Gr70,” *Caspian Journal of Applied Sciences Research*, vol. 1, no. 5, pp. 41–47, 2012.
- [20] S. Zheng, C. Chen and L. Chen, “Influence of S Contents on the Hydrogen Blistering and Hydrogen Induced Cracking of A350LF2 Steel,” *Mater. Sci. Appl.*, vol. 2, no. 7, pp. 917–921, 2011.
- [21] S. N. Smith and W. Michael, “Corrosion of carbon steel by H₂S in CO₂ containing oil field Environments,” *NACE Int.*, Paper No.06115, 2006.
- [22] J. T. Report, “Corrosion resistant high Cr steel for oil and gas wells,” *JFE Tech. Rep.*, no. 18, pp. 63–65, 2013.
- [23] NACE, *ISO 15156-2: Petroleum and natural gas industries — Materials for use in H₂S-containing environments in oil and gas production*, 2009.
- [24] H. Kurahashi, T. Kurisu, Y. Sone, K. Wada, and Y. Nakai, “Stress Corrosion Cracking of 13Cr Steels in CO₂ H₂S-CI Environments,” *Corrosion*, vol. 41, no. 4, pp. 211–219, 1985.
- [25] P. Patnaik, *A Comprehensive Guide to the Hazardous Properties of Chemical Substances*. Wiley, Third Edition, 2007.
- [26] L. Skrtic, “Hydrogen Sulfide, Oil and Gas, and People’s Health,” *Energy*, pp. 1–77, May, 2006.
- [27] J. G. Speight, “Fuel Science and Technology Handbook,” in *Fuel Science and Technology*

- Handbook*, New York: Marcel Dekker, 1990, pp. 137–149.
- [28] K. O. Xue, M. R. Chitrakar and K. Sakane, “Screening of Adsorbents for Removal of H₂S at Room Temperature,” *Green Chemistry*, Issue 5, 2003.
- [29] W. Sun and S. Nestic, “A Mechanistic Model of H₂S Corrosion of Mild Steel,” *NACE Int. - Corros. Conf. Expo*, no. 7655, 2007.
- [30] J. Kvarekva. J. Amri, “Simulation of Solid-state Growth of Iron Sulfide in Sour Corrosion Conditions,” *NACE Corros.*, Paper No.11078, 2011.
- [31] D. P. Li, L. Zhang, J. W. Yang, M. X. Lu, J. H. Ding, and M. L. Liu, “Effect of H₂S concentration on the corrosion behavior of pipeline steel under the coexistence of H₂S and CO₂,” *Int. J. Miner. Metall. Mater.*, vol. 21, no. 4, pp. 388–394, 2014.
- [32] M. L. Zhang, W. Zhong, J. Yang and T. Gu, X. Xiao, “Effects of Temperature and Partial Pressure on H₂S/CO₂ Corrosion of Pipeline Steel in Sour Conditions,” *Corrosion*, Paper No. 11079, 2011.
- [33] A. L. Young and R. C. John, “New Understanding on Corrosion of Alloys in High-Temperature Sulfidizing Gases,” *Corrosion*, Paper No. 02486, 2002.
- [34] L. N. Houyi Ma, Cheng Xiaoliang and Guiqiu Li, “The influence of hydrogen sulfide on corrosion of iron under different conditions,” *Corros. Sci.*, pp. 1669–1683, 1999.
- [35] D. W. Shoesmith, “The Formation of Ferrous Monosulfide Polymorphs during the Corrosion of Iron by Aqueous Hydrogen Sulfide at 21°C,” *J. Electrochem. Soc.*, vol. 127, no. 5, p. 1007, 1980.
- [36] L. Khaksar and J. Shirokoff, “Effect of elemental sulfur and sulfide on the corrosion

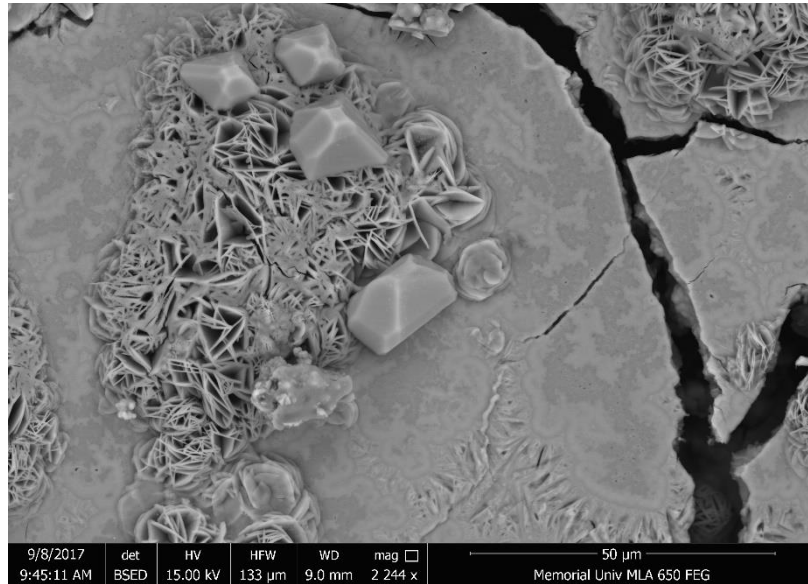
- behavior of Cr-Mo low alloy steel for tubing and tubular components in oil and gas industry,” *Materials (Basel)*, vol. 10, no. 4, 2017.
- [37] L. Khaksar, G. Whelan and J. Shirokoff, “Electrochemical and microstructural analysis of FeS films from acidic chemical bath at varying temperatures, pH, and Immersion Time,” *Int. J. Corros.*, 2016.
- [38] M. Koteeswaran, “CO₂ and H₂S Corrosion in Oil Pipelines,” M.S. Thesis, Faculty of Mathematics and Natural Science, University of Stavanger, Norway, June, 2010.
- [39] S. N. Smith, “Predicting Corrosion in Slightly Sour Environments,” *Mater. Perform. - Mater. Sel. Desing*, no. 241, pp. 60–64, 2002.
- [40] J. S. Smith and J. D. A. Miller, “Nature of Sulphides and Their Corrosive Effect on Ferrous Metals: A Review,” *Br. Corros. J.*, vol. 10, no. 3, pp. 136–143, 1975.
- [41] R. A. Berner, “Thermodynamic Stability of Sedimentary Iron Sulfides,” *American Journal Science.*, vol. 265, pp. 773–785, 1967.
- [42] R. G. Arnold and L. E. Reichen, “Measurement of the Metal Content of Naturally Occurring, Metal-Deficient, Hexagonal Pyrrhotite by an X-ray Spacing Method,” *Am. Mineral.*, vol. 47, pp. 105–112, 1962.
- [43] B. J. Skinner, R. C. Erd and F. S. Grimaldi “Greigite, the Thio-spinel of Iron; A New Mineral,” *Am. Mineral.*, vol. 49, pp. 543–555, 1964.
- [44] J. A. Morice, L. V. C. Rees. and D. T. Rickard, “Mössbauer Studies of Iron Sulphides,” *Inorg. Nucl. Chem.*, vol. 31, pp. 3797–3802, 1969.
- [45] F. Pessu, R. Barker, and A. Neville, “Early stages of pitting corrosion of UNS K03014

- carbon steel in sour corrosion environments : The influence of CO₂ , H₂S and temperature.,” *NACE Int. - Corros. Conf. Expo*, Paper no. 5583, 2015.
- [46] W. Sun, D. V Pugh, and R. J. Franco, “A Parametric Study of Sour Corrosion of Carbon Steel,” *NACE Int.*, Paper no. 10278, pp. 1–20, 2010.
- [47] A. I. Almarshad and D. Jamal, “Electrochemical Investigations of Pitting Corrosion Behaviour of Type UNS S31603 Stainless Steel in Thiosulfate-Chloride Environment,” *J. Appl. Electrochem.*, vol. 34, no. 1, pp. 67–70, 2004.
- [48] Pourbaix. Marcel, “Atlas of Electrochemical Equilibria in Aqueous Solutions.,” *NACE Int.*, 1966.
- [49] M. Saeed Akhtar, A. Alenad, and M. Azad Malik, “Synthesis of mackinawite FeS thin films from acidic chemical baths,” *Mater. Sci. Semicond. Process.*, vol. 32, pp. 1–5, 2015.
- [50] F. Mansfeld, H. Shih, C.H.Tsai, and H. Greene, “Analysis of EIS Data for Common Corrosion Processes,” *Am. Soc. Test. Mater.*, vol. 1188, pp. 37–53, 1993.
- [51] Wei Sun and Srdjan Nesic., “Kinetics of Iron sulphide and Mixed Iron Sulphide / Carbonate scale precipitation in CO₂/H₂S Corrosion.” *Corrosion*, Paper No. 06644, 2006
- [52] K. Lee, “A mechanistic modeling of CO₂ corrosion of mild steel in the presence of H₂S,” Ph.D. Thesis, Russ College of Engineering and Technology of Ohio Univeristy, November, 2004.
- [53] H. Ma *et al.*, “The influence of hydrogen sulfide on corrosion of iron under different conditions,” *Corros. Sci.*, vol. 42, no. 10, pp. 1669–1683, 2000.
- [54] W. Sun, S. Nešić, and S. Papavinasam, “Kinetics of corrosion layer formation. Part 2 - Iron

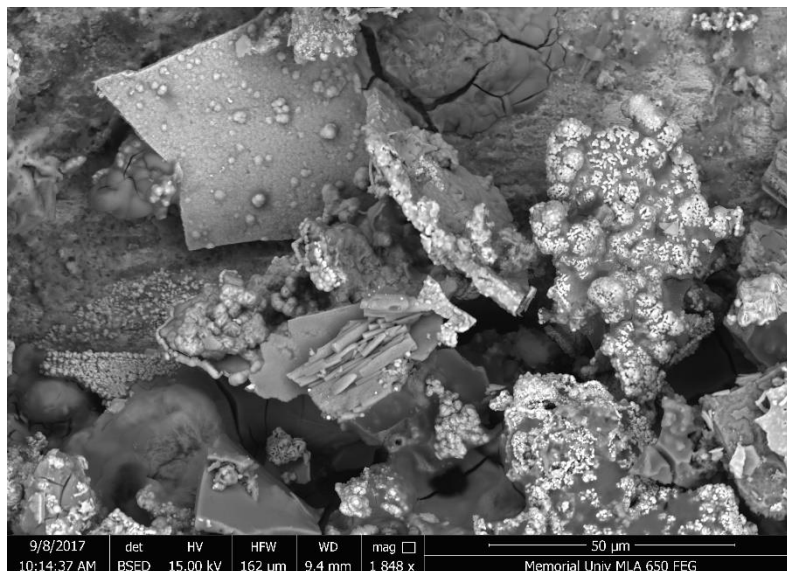
- sulfide and mixed iron sulfide/carbonate layers in carbon dioxide/hydrogen sulfide corrosion,” *Corrosion*, vol. 64, no. 7, pp. 586–599, 2008.
- [55] J. Han, Y. Yang, S. Netic, and B. N. Brown, “Roles of Passivation and Galvanic Effects in,” *Corros. 2008*, Paper no. 08332, pp. 1–19, 2008.
- [56] Hemmingsen T, Hilbert L, and Nielsen L.V, “Assessment of sulphur and H₂S corrosion by use of simultaneous ER, galvanic and optical measurements.,” *Eurocorr*, 2003.
- [57] David R.B, “Sodium Sulfides,” *Kirk-Othmer Encycl. Chem. Technol.*, 1997.
- [58] D. G. Enos and L. L. Scribner, “The Potentiodynamic Polarization Scan” Technical Report 33,” *Cent. Electrochem. Sci. Eng.*, pp. 1–13, 1997.
- [59] M. Corrales-Luna, *et al.*, “Influence of the immersion time and temperature on the corrosion of API X52 steel in an aqueous salt medium,” *Int. J. Electrochem. Sci.*, vol. 12, no. 7, pp. 6729–6741, 2017.
- [60] S. N. Smith, “A proposed mechanism for corrosion in slightly sour oil and gas production,” *NACE*, September, 1993, pp. 2695–2706.
- [61] D. Brondel, R. Edwards, A. Hayman, D. Hill, and T. Semerad, “Corrosion in the Oil Industry,” *Oilf. Rev.*, pp. 4–18, 1994.
- [62] K. J. Lee and S. Netic, “The Effect of Trace Amount of H₂S and CO₂ Corrosion Investigated by Using the EIS technique,” *Spectroscopy*, no. 5630, pp. 1–16, 2005.
- [63] M.B. Kermani, G. Weighhill and T. Pendlington, “Operational experience of using 13%Cr tubular steels,” *NACE Int.*, 1995.
- [64] D.G. Enos and L.L. Scribner, “Potentiodynamic Polarisation Scan,” *Technical Report 33.*,

University of Virginia, January, 1997.

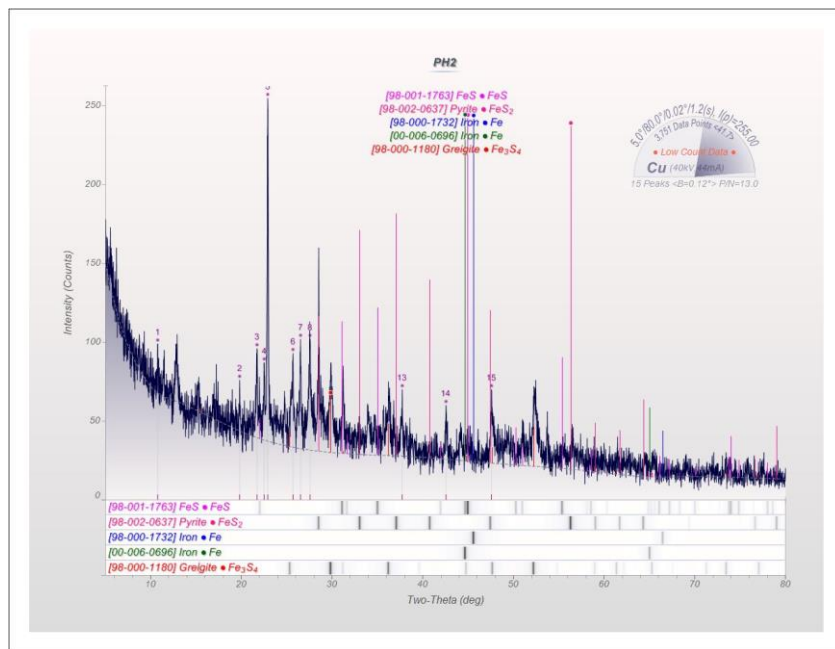
APPENDIX



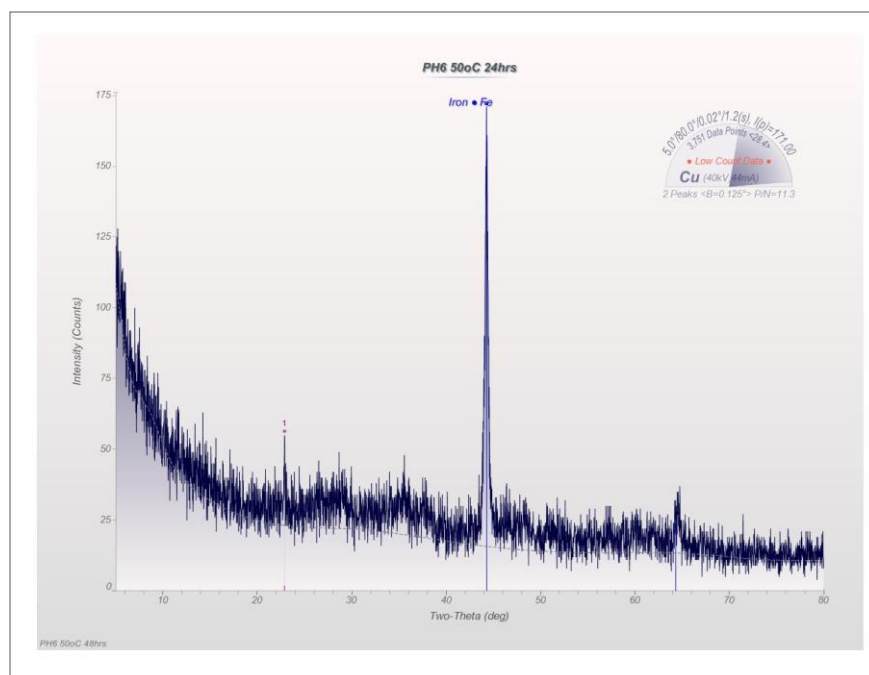
SEM image of the experimental sample at conditions; temperature 50°C, pH 6 and Immersion time of 24 hours.



SEM image of the experimental sample at conditions; temperature 40°C, pH 2 and Immersion time of 72 hours.



XRD analysis of the corrosion product formed on the steel surface at: 70°C, pH2 and 24 hours.



XRD analysis of the corrosion product formed on the steel surface at: 50°C, pH6 and 48 hours.

Phase Info - Iron 98-001-9698

Iron
Fe

Powder Pattern (Calculated)

Radiation: Cu (K α 1) λ : 1.54059 Å Filter:
 Calibration: 2 θ : 114.536° Lines: 5 RIR: 11.61
 Reference: Calculated from CSD#19698 in AMCSO @7/9/2014 11:42:04 AM

Unit Cell Data ()

Crystal System: Cubic S.G: Im3m (229) Z: 2 P.S: cI2
 Lattice Constants: 2.8970, 2.8970, 2.8970 (Å) <90.00°, 90.00°, 90.00°>
 Volume: 24.3 Density: 7.628 Mwt: F(30):
 Reference: Basinski Z S Hume-Rothery W Sutton A L, Proceedings of the Royal Society of London vA229 (1955) p459-467,
 The lattice expansion of iron Sample: at T = 1175 K • AMCSO#0015346



#	Angle	d(Å)	I%(f)	(h k l)	2 π /d	#	Angle	d(Å)	I%(f)	(h k l)	2 π /d
1	44.256	2.0485	100.0	(1 1 0)	3.0672						
2	64.333	1.4485	13.7	(2 0 0)	4.3377						
3	81.360	1.1827	24.5	(2 1 1)	5.3126						
4	97.619	1.0242	7.7	(2 2 0)	6.1345						
5	114.536	0.9161	13.4	(3 1 0)	6.8585						

Phase information of the corrosion product formed on the steel surface during XRD (IRON (Fe), PDF# 98-001-9698).

Phase Info - Iron Sulfide

03-065-1894

Iron Sulfide**FeS**

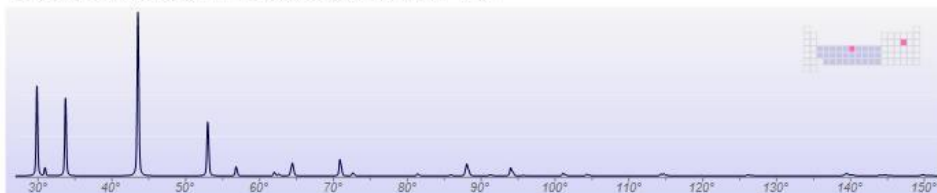
Powder Pattern (QM: Indexed, Calculated)

Radiation: CuK α 1 λ : 1.5406 Å Filter:
 Calibration: 2 θ : 149.817° Lines: 35 RIR: 4.39
 Reference: Calculated from NIST using POWD-12++

Unit Cell Data ()

Crystal System: Hexagonal S.G: P63/mmc (194) Z: 2 P.S: hP4
 Lattice Constants: 3.4559, 3.4559, 5.7789 (Å) <90.00°, 90.00°, 120.00°>
 Volume: 59.8 Density: 4.884 Mwt: 87.91 F(30): 999.9 (0.0002,32/0)
 Reference: E.J.Fasiska, Phys. Status Solidi A, vA10 p169 (1972)

NIST M&A collection code: N AL5030 4191. Temperature Factor: IB=Fe,S. Minor Warning: No Rfactor reported/abstracted.
 Prototype Structure: Ni As LPF Prototype Structure: Ni As,hP4,194



#	Angle	d(Å)	I%(f)	(h k l)	2 π /d	#	Angle	d(Å)	I%(f)	(h k l)	2 π /d
1	29.829	2.9929	49.5	(1 0 0)	2.0994	25	114.727	0.9147	1.6	(2 0 5)	6.8690
2	30.923	2.8895	4.5	(0 0 2)	2.1745	26	119.732	0.8907	0.4	(2 1 4)	7.0545
3	33.697	2.6576	43.9	(1 0 1)	2.3642	27	126.143	0.8640	1.7	(2 2 0)	7.2724
4	43.500	2.0788	100.0	(1 0 2)	3.0226	28	132.586	0.8413	0.1	(1 1 6)	7.4685
5	52.947	1.7280	35.8	(1 1 0)	3.6362	29	136.243	0.8301	0.1	(3 1 0)	7.5694
6	56.790	1.6198	6.3	(1 0 3)	3.8790	30	137.049	0.8278	0.1	(2 2 2)	7.5906
7	61.961	1.4965	2.7	(2 0 0)	4.1987	31	139.272	0.8216	1.8	(3 1 1)	7.6471
8	62.586	1.4830	1.3	(1 1 2)	4.2368	32	139.544	0.8209	3.0	(3 0 4)	7.6538
9	64.244	1.4487	4.3	(2 0 1)	4.3372	33	144.017	0.8099	1.4	(2 0 6)	7.7580
10	64.441	1.4447	7.0	(0 0 4)	4.3490	34	144.662	0.8084	1.4	(2 1 5)	7.7721
11	70.857	1.3288	12.7	(2 0 2)	4.7284	35	149.817	0.7978	2.9	(3 1 2)	7.8755
12	72.605	1.3011	2.4	(1 0 4)	4.8292						
13	81.358	1.1818	1.8	(2 0 3)	5.3168						
14	85.836	1.1312	0.9	(2 1 0)	5.5544						
15	87.875	1.1101	3.4	(2 1 1)	5.6598						
16	88.052	1.1084	8.6	(1 1 4)	5.6689						
17	91.195	1.0782	1.1	(1 0 5)	5.8276						
18	93.987	1.0534	7.7	(2 1 2)	5.9649						
19	95.652	1.0394	0.5	(2 0 4)	6.0451						
20	101.090	0.9976	2.7	(3 0 0)	6.2981						
21	104.312	0.9755	1.8	(2 1 3)	6.4413						
22	106.216	0.9632	0.1	(0 0 6)	6.5236						
23	109.541	0.9430	0.1	(3 0 2)	6.6629						
24	114.314	0.9168	2.0	(1 0 6)	6.8531						

September-08-17, 2:19 PM • Memorial Univ - NL

Phase information of the corrosion product formed on the steel surface during XRD (IRON SULPHIDE (FeS), PDF# 03-065-1894).

Phase Info - Pyrite 00-042-1340

Pyrite



Powder Pattern (QM: Star, Diffractometer)

Radiation: CuKα1 λ: 1.540598 Å Filter: Graph CAS#: 1309-36-0
 Calibration: Internal (Si) 2θ: 119.72° Lines: 27 RIR: 1.60

Reference: Nodland, D., Syvinski, W., McCarthy, G., *Bayliss, P., North Dakota State Univ., Fargo, North Dakota, USA., ICDD Grant-in-Aid (1989)

Unit Cell Data (Powder Diffraction)

Crystal System: Cubic S.G: Pa-3 (205) Z: 4 P.S: cP12

Lattice Constants: 5.4179, 5.4179, 5.4179 (Å) <90.00°, 90.00°, 90.00°>

Volume: 159.0 Density: 5.010 Mwt: 119.97 F(27): 97.8 (0.0095,29/0)

Reference: Brostigen, G., Kjekshus, A., Acta Chem. Scand., v23 p2186 (1969)

Additional Patterns: Validated by calculated pattern 00-024-0076. To replace 00-006-0710. See PDF 01-071-0053. Analysis: Microprobe analysis (wt.%): Fe 46.8, S 53.5: "Fe S2". Color: Yellow metallic. General Comments: (*)Department of Geology and Geophysics, University of Calgary, Alberta, Canada. Sample Source or Locality: Specimen from Itaya mine, Yamagata Prefecture, Japan. Prototype Structure: Fe S2



#	Angle	d(Å)	I%(f)	(h k l)	2π/d	#	Angle	d(Å)	I%(f)	(h k l)	2π/d
1	28.512	3.1280	31.0	(1 1 1)	2.0087	23	107.089	0.9577	12.0	(4 4 0)	6.5607
2	33.084	2.7055	100.0	(2 0 0)	2.3224	24	109.508	0.9432	0.0	(4 4 1)	6.6616
3	37.106	2.4209	53.0	(2 1 0)	2.5954	25	114.515	0.9158	2.0	(5 3 1)	6.8608
4	40.784	2.2107	40.0	(2 1 1)	2.8422	26	117.084	0.9030	6.0	(4 4 2)	6.9580
5	47.411	1.9160	36.0	(2 2 0)	3.2793	27	119.720	0.8907	2.0	(6 1 0)	7.0541
6	50.491	1.8061	1.0	(2 2 1)	3.4789						
7	56.279	1.6333	69.0	(3 1 1)	3.8469						
8	59.016	1.5639	11.0	(2 2 2)	4.0176						
9	61.694	1.5023	13.0	(0 2 3)	4.1824						
10	64.283	1.4479	16.0	(3 2 1)	4.3395						
11	71.772	1.3141	1.0	(4 1 0)	4.7814						
12	74.200	1.2770	0.0	(4 1 1)	4.9203						
13	76.597	1.2429	6.0	(3 3 1)	5.0553						
14	78.959	1.2115	7.0	(4 2 0)	5.1862						
15	81.316	1.1823	7.0	(1 2 4)	5.3146						
16	83.639	1.1552	3.0	(3 3 2)	5.4389						
17	88.291	1.1060	7.0	(4 2 2)	5.6811						
18	90.632	1.0834	0.0	(4 3 0)	5.7995						
19	92.932	1.0625	0.0	(4 3 1)	5.9134						
20	95.248	1.0427	20.0	(3 3 3)	6.0258						
21	99.917	1.0062	7.0	(2 3 4)	6.2447						
22	102.287	0.9892	4.0	(1 2 5)	6.3519						

September-08-17, 2:18 PM • Memorial Univ - NL

Phase information of the corrosion product formed on the steel surface during XRD (PYRITE (FeS₂), PDF# 00-042-1340).

Phase Info - Greigite

00-016-0713

Greigite

Powder Pattern (QM: Indexed, Diffractometer)

Radiation: FeK α λ : 1.9373 Å Filter:
 Calibration: Internal (Si) 2 θ : 99.668° Lines: 27 RIR:
 Reference: Skinner, Erd, R., Grimaldi, Am. Mineral., v49 p543 (1964)

Unit Cell Data (Powder Diffraction)

Crystal System: Cubic S.G: Fd-3m (227) Z: 8 P.S: cF56
 Lattice Constants: 9.8760, 9.8760, 9.8760 (Å) <90.00°, 90.00°, 90.00°>
 Volume: 963.3 Density: 4.049 Mwt: 295.78 F(27): 12.1 (0.074,30/0)
 Reference: Ibid.

Additional Patterns: To replace 00-023-1122. Color: Black. General Comments: Measured density on specimen from Zacatecas.
 Sample Preparation: Cell dimension determined from 440 reflection at 25 C using Si as internal standard. Sample Source or
 Locality: Specimen from clay layers in Lake sediments, Kramer-Four Corners area, San Bernardino County, California, USA.
 Warning: Lines with abs(delta 2Theta)>0.06 DEG. Prototype Structure: Mg Al2 O4



#	Angle	d(Å)	I%(f)	(h k l)	2 π /d	#	Angle	d(Å)	I%(f)	(h k l)	2 π /d
1	15.479	5.7200	8.0	(1 1 1)	1.0985	23	88.379	1.1051	16.0	(8 4 0)	5.6856
2	25.428	3.5000	30.0	(2 2 0)	1.7952	24	90.526	1.0844	0.0	(9 1 1)	5.7942
3	29.961	2.9800	100.0	(3 1 1)	2.1085	25	93.866	1.0544	2.0	(6 6 4)	5.9590
4	31.305	2.8550	4.0	(2 2 2)	2.2008	26	96.177	1.0351	8.0	(9 3 1)	6.0701
5	36.343	2.4700	55.0	(4 0 0)	2.5438	27	99.668	1.0080	30.0	(8 4 4)	6.2333
6	39.856	2.2600	2.0	(3 3 1)	2.7802						
7	44.903	2.0170	10.0	(4 2 2)	3.1151						
8	47.808	1.9010	30.0	(5 1 1)	3.3052						
9	52.358	1.7460	75.0	(4 4 0)	3.5986						
10	54.901	1.6710	0.0	(5 3 1)	3.7601						
11	59.074	1.5625	10.0	(6 2 0)	4.0212						
12	61.535	1.5058	10.0	(5 3 3)	4.1727						
13	62.338	1.4883	2.0	(6 2 2)	4.2217						
14	65.428	1.4253	8.0	(4 4 4)	4.4083						
15	67.716	1.3826	0.0	(7 1 1)	4.5445						
16	71.377	1.3204	4.0	(6 4 2)	4.7585						
17	73.601	1.2859	12.0	(7 3 1)	4.8862						
18	77.184	1.2349	10.0	(8 0 0)	5.0880						
19	79.102	1.2097	0.0	(7 3 3)	5.1940						
20	80.070	1.1975	0.0	(6 4 4)	5.2469						
21	82.869	1.1640	0.0	(8 2 2)	5.3979						
22	85.007	1.1401	2.0	(7 5 1)	5.5111						

September-08-17, 2:34 PM • Memorial Univ - NL

Phase information of the corrosion product formed on the steel surface during XRD (GREIGITE
 (Fe₃S₄), PDF# 00-016-0713).

Phase Info - Pyrrhotite

98-000-1338

Pyrrhotite

Powder Pattern (Calculated)

Radiation: Cu (Kα1) λ: 1.54059 Å Filter:
 Calibration: 2θ: 91.896° Lines: 207 RIR: 1.33
 Reference: Calculated from CSD#1338 in AMCSDB @7/9/2014 11:42:04 AM

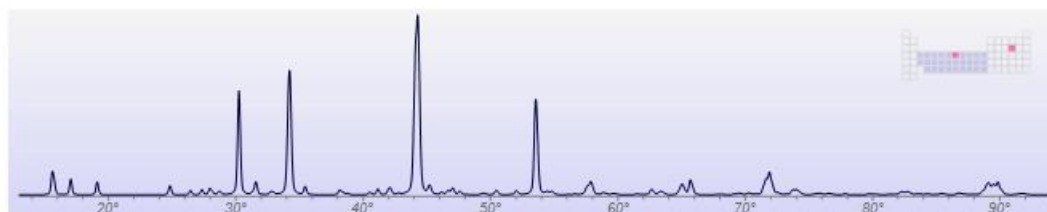
Unit Cell Data ()

Crystal System: Monoclinic S.G: F2/d (15) Z: 8 P.S: mF120

Lattice Constants: 11.9020, 6.8590, 22.7870 (Å) <90.00°, 90.43°, 90.00°>

Volume: 1860.2 Density: 4.623 Mwt: F(30):

Reference: Tokonami M Nishiguchi K Morimoto N, American Mineralogist v57 (1972) p1066-1080, Crystal structure of a monoclinic pyrrhotite (Fe₇S₈) • AMCSDB#0000288



#	Angle	d(Å)	I%(I)	(h k l)	2π/d	#	Angle	d(Å)	I%(I)	(h k l)	2π/d
1	15.572	5.7557	14.3	(-1 1 1)	1.0917	27	34.138	2.6386	69.9	(-2 2 4)	2.3813
2	15.601	5.7452	3.8	(1 1 1)	1.0937	28	34.262	2.6293	68.3	(4 0 4)	2.3897
3	15.733	5.6966	9.0	(0 0 4)	1.1030	29	35.422	2.5453	7.9	(0 2 6)	2.4686
4	16.933	5.2910	0.9	(-2 0 2)	1.1875	30	38.120	2.3702	4.5	(-3 1 7)	2.6509
5	17.037	5.2585	13.4	(2 0 2)	1.1949	31	38.377	2.3549	2.7	(3 1 7)	2.6682
6	19.101	4.6889	10.9	(-1 1 3)	1.3400	32	38.698	2.3360	0.3	(2 2 6)	2.6898
7	19.170	4.6719	0.8	(1 1 3)	1.3449	33	38.759	2.3324	1.3	(-1 1 9)	2.6939
8	24.742	3.6229	1.8	(-1 1 5)	1.7343	34	40.428	2.2394	1.0	(-5 1 1)	2.8057
9	24.832	3.6098	7.2	(1 1 5)	1.7406	35	40.527	2.2342	1.9	(1 3 1)	2.8123
10	26.386	3.3991	1.0	(-3 1 1)	1.8485	36	41.039	2.2073	0.3	(-4 2 2)	2.8465
11	26.438	3.3926	3.1	(3 1 1)	1.8520	37	41.131	2.2026	5.7	(4 2 2)	2.8526
12	27.322	3.2839	4.9	(0 2 2)	1.9133	38	41.967	2.1604	4.4	(-5 1 3)	2.9083
13	27.939	3.2123	5.6	(-2 0 6)	1.9560	39	42.097	2.1540	0.4	(-1 3 3)	2.9170
14	28.132	3.1905	2.3	(2 0 6)	1.9693	40	42.131	2.1523	4.5	(1 3 3)	2.9192
15	28.621	3.1368	1.8	(-3 1 3)	2.0030	41	42.746	2.1227	1.3	(2,0,10)	2.9601
16	28.762	3.1216	2.2	(3 1 3)	2.0128	42	43.342	2.0947	0.3	(-4 2 4)	2.9996
17	30.198	2.9754	35.1	(4 0 0)	2.1117	43	43.988	2.0653	48.8	(-4 0 8)	3.0423
18	30.240	2.9714	65.6	(2 2 0)	2.1146	44	44.106	2.0600	99.0	(-2 2 8)	3.0500
19	31.241	2.8778	1.1	(-2 2 2)	2.1833	45	44.279	2.0523	100.0	(2 2 8)	3.0615
20	31.299	2.8726	0.3	(2 2 2)	2.1873	46	44.335	2.0499	50.7	(4 0 8)	3.0652
21	31.445	2.8595	1.9	(-1 1 7)	2.1973	47	44.463	2.0442	0.3	(-3 1 9)	3.0736
22	31.547	2.8505	4.2	(1 1 7)	2.2043	48	44.969	2.0223	0.3	(-5 1 5)	3.1069
23	31.571	2.8483	7.0	(0 0 8)	2.2059	49	45.135	2.0152	4.6	(-1 3 5)	3.1178
24	32.708	2.7512	2.4	(-3 1 5)	2.2838	50	45.188	2.0130	0.4	(1 3 5)	3.1213
25	32.918	2.7341	2.1	(3 1 5)	2.2981	51	45.235	2.0110	4.6	(5 1 5)	3.1245
26	34.046	2.6455	17.2	(-4 0 4)	2.3751	52	46.124	1.9741	2.3	(-3 3 1)	3.1828

June-28-17, 2:26 PM • Memorial Univ - NL

Phase information of the corrosion product formed on the steel surface during XRD (PYRRHOTITE (Fe₇S₈), PDF# 98-000-1338).